NASA TECHNICAL MEMORANDUM

NASA TM X-72697

COPY NO.____

NASA TM X-72697

LOW-SPEED AERODYNAMIC CHARACTERISTICS OF A 13-PERCENT-THICK AIRFOIL SECTION DESIGNED FOR GENERAL AVIATION APPLICATIONS

By Robert J. McGhee, William D. Beasley, and Dan M. Somers

RELEASED FOR PUBLIC AVAILABILITY
MAY 2, 1977

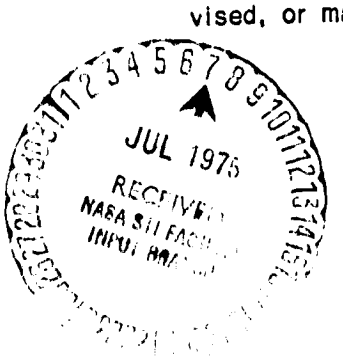

NATIONAL AERONAUTICS AND SPACE ADMINISTRATION
LANGLEY RESEARCH CENTER, HAMPTON, VIRGINIA 23665

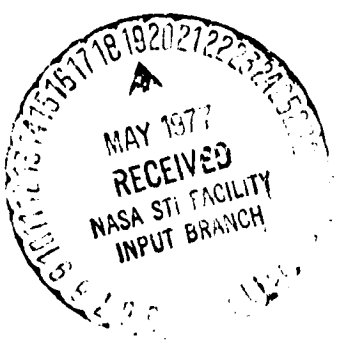

LOW-SPEED AERODYNAMIC CHARACTERISTICS OF A 13-PERCENT-THICK AIRFOIL SECTION DESIGNED FOR GENERAL AVIATION APPLICATIONS

By Robert J. McGhee, William D. Beasley, and Dan M. Somers

Langley Research Center

SUMMARY

An investigation was conducted in the Langley low-turbulence pressure tunnel to determine the low-speed section characteristics of a 13-percent-thick airfoil designed for general aviation applications. The results are compared with older NACA 12-percent-thick sections and with the 17-percent-thick NASA GA(W)-1 airfoil. The tests were conducted over a Mach number range from 0.10 to 0.35 and an angle-of-attack range from -10° to 22°. Chord Reynolds numbers were varied from about 2.0×10^6 to 9.0×10^6.

The results of the investigation indicate that maximum section lift coefficients at a Mach number of 0.15 increased from about 1.7 to 2.1 as the Reynolds number was increased from about 2.0×10^6 to 9.0×10^6. Stall characteristics were generally gradual and of the trailing-edge type. The application of a narrow roughness strip near the leading edge resulted in only small effects on the lift characteristics at a Reynolds number of about 6.0×10^6, whereas extensive roughness wrapped around the leading-edge resulted in a decrease in maximum section lift coefficient of about 19 percent. Increasing the Mach number from 0.10 to 0.35 at a constant Reynolds number of about 6.0×10^6 decreased the maximum section lift coefficient about 16 percent, with most of the decrease occurring above a Mach number of about 0.28. The 13-percent-thick

airfoil compared to the 17-percent-thick GA(W)-1 airfoil, provided about a 0.10 increase in maximum section lift coefficient, reduced the section profile drag coefficients at all lift coefficients, and increased the section lift-drag ratio about 22 percent at cruise and about 14 percent at climb. Maximum section lift coefficient at a Reynolds number of about 6.0×10^6 was about 16 percent greater than the NACA 23012 airfoil section.

INTRODUCTION

Research on advanced technology airfoils has received considerable attention over the last several years at the Langley Research Center. Reference 1 reports the results of the NASA GA(W)-1 airfoil, which was specifically designed for a twin-engine propeller driven light airplane. The achievement of high performance of the GA(W)-1 airfoil has prompted the development of a family of airfoils of differing thickness and camber. This report presents the basic low-speed aerodynamic characteristics of a 13-percent-thick airfoil derived from the GA(W)-1 airfoil. This airfoil has been designated as General Aviation (Whitcomb)-number two airfoil. (GA(W)-2).

The investigation was performed in the Langley low-turbulence pressure tunnel over a Mach number range from 0.10 to 0.35. The chord Reynolds number varied from about 2.0×10^6 to 9.0×10^6. The geometrical angle of attack varied from about -10° to 22°.

SYMBOLS

Values are given in both SI and the U.S. Customary Units. The measurements and calculations were made in the U.S. Customary Units.

C_p pressure coefficient, $\frac{p_L - p_\infty}{q_\infty}$

c airfoil chord, centimeters (inches)

c_c section chord-force coefficient, $\oint c_p \, d\left(\frac{z}{c}\right)$

c_d section profile-drag coefficient, $\int_{\text{wake}} c'_d \, d\left(\frac{h}{c}\right)$

c'_d point drag coefficient (ref. 2)

c_l section lift coefficient, $c_n \cos \alpha - c_c \sin \alpha$

c_m section pitching-moment coefficient about quarter-chord point,

$$-\oint c_p \left(\frac{x}{c} - 0.25\right) d\left(\frac{x}{c}\right) + \oint c_p \left(\frac{z}{c}\right) d\left(\frac{z}{c}\right)$$

c_n section normal-force coefficient, $-\oint c_p \, d\left(\frac{x}{c}\right)$

h vertical distance in wake profile, centimeters (inches)

l/d section lift-drag ratio, c_l / c_d

M free-stream Mach number

p static pressure, N/m^2 (lb/ft^2)

q dynamic pressure, N/m^2 (lb/ft^2)

R Reynolds number based on free-stream conditions and airfoil chord

t airfoil thickness, centimeters (inches)

x airfoil abscissa, centimeters (inches)

z airfoil ordinate, centimeters (inches)

z_c mean line ordinate, centimeters (inches)

z_t mean thickness, centimeters (inches)

α geometric angle of attack, degrees

Subscripts:

L local point on airfoil

max maximum

∞ free-stream conditions

MODEL, APPARATUS, AND PROCEDURE

Model

The 13-percent airfoil section (fig. 1) was obtained by linearly decreasing the mean thickness distribution of the 17-percent GA(W)-1 airfoil by 0.765 $\left(\frac{13}{17}\right)$ and combining this thickness distribution with the mean camber line of the GA(W)-1 airfoil. This method of obtaining the airfoil family was selected after theoretical analysis, using a subsonic viscous method, showed that the resulting airfoils should have similar characteristics to the GA(W)-1 airfoil. The mean camber and thickness distribution are shown in figure 2 and table I presents the measured airfoil coordinates.

The airfoil model was constructed utilizing a metal core around which plastic fill and two thin layers of fiberglass was used to form the contour of the airfoil. The model had a chord of 61.01 cm (24.02 in.) and a span of 91.44 cm (36 in.). The model was equipped with both upper and lower surface orifices located 5.08 cm (2 in.) off the midspan and at the chord stations indicated in table II. The airfoil surface was sanded in the chordwise direction with number 400 dry silicon carbide paper to provide a smooth aerodynamic finish. Figure 3 shows a photograph of the model.

Wind Tunnel

The Langley low-turbulence pressure tunnel (ref. 3) is a closed-throat, single-return tunnel which can be operated at stagnation pressures from 1 to 10 atmospheres with tunnel-empty test section Mach numbers up to 0.42 and 0.22, respectively. The maximum unit Reynolds number is about 49×10^6 per meter (15×10^6 per foot) at a Mach number of about 0.22. The tunnel test section is 91.44 cm (3 ft) wide by 228.6 (7.5 ft) high.

Hydraulically actuated circular plates provided positioning and attachment for the two-dimensional model. The plates are 101.60 cm (40 in.) in diameter, rotate with the airfoil, and are flush with the tunnel wall. The airfoil ends were attached to rectangular model attachment plates (fig. 4) and the airfoil was mounted so that the center of rotation of the circular plates was at 0.25c on the model reference line. The air gaps at the tunnel walls between the rectangular plates and the circular plates were sealed with flexible sliding metal seals, shown in figure 4.

Wake Survey Rake

A fixed wake survey rake (fig. 5) at the model midspan was cantilever mounted from the tunnel sidewall and located one chord length behind the trailing edge of the airfoil. The wake rake utilized 91 total-pressure tubes, 0.1524 cm (0.060 in.) in diameter, and six static-pressure tubes, 0.3175 cm (0.125 in.) in diameter. The total-pressure tubes were flattened to 0.1016 cm (0.040 in.) for 0.6096 cm (0.24 in.) from the tip of the tube. The static-pressure tubes each had four flush orifices drilled 90° apart and located 8 tube diameters from the tip of the tube and in the measurement plane of the total-pressure tubes.

Instrumentation

Measurements of the static pressures on the airfoil surfaces and the wake rake pressures were made by an automatic pressure-scanning system utilizing variable-capacitance-type precision transducers. Basic tunnel pressures were measured with precision quartz manometers. Angle of attack was measured with a calibrated digital shaft encoder operated by a pinion gear and rack attached to the circular model attachment plates. Data were obtained by a high-speed acquisition system and recorded on magnetic tape.

TESTS AND METHODS

The airfoil was tested at Mach numbers from 0.10 to 0.35 over an angle-of-attack range from about -10° to 22°. Reynolds number based on the airfoil chord was varied from about 2.0×10^6 to 9.0×10^6. The airfoil was tested both smooth (natural transition) and with roughness located on both upper and lower surfaces at 0.075c. The roughness was sized for each Reynolds number according to reference 4. The roughness consisted of granular-type strips 0.127 cm (0.05 in.) wide, sparely distributed, and attached to the airfoil surface with clear lacquer. At a Reynolds number of 6.0×10^6 and a Mach number of 0.15 the NACA standard roughness (number 60 grains wrapped around leading edge on both surfaces back to 0.08c) was employed so that comparisons with older NACA airfoil data could be made. For several test runs oil was spread over the airfoil upper surface to determine if any local flow separation was present. Tufts were attached to the airfoil and tunnel sidewalls with plastic tape to determine stall patterns.

The static-pressure measurements at the airfoil surface were reduced to standard pressure coefficients and machine integrated to obtain section normal-force and chord-force coefficients and section pitching-moment coefficients about the quarter chord. Section profile-drag coefficient was computed from the wake-rake total and static pressures by the method reported in reference 2.

An estimate of the standard low-speed wind-tunnel boundary corrections (ref. 5) amounted to a maximum of about 2 percent of the measured coefficients and these corrections have not been applied to the data, except for the data shown in figure 18(a).

PRESENTATION OF DATA

DISCUSSION

Lift.- Figure 6 shows that with the GA(W)-2 airfoil smooth (natural boundary-layer transition) a lift-curve slope of about 0.11 per degree (uncorrected for wall boundary effects) and a lift coefficient of about 0.49 at $\alpha = 0°$ was obtained for the Reynolds numbers investigated, (M = 0.15). Maximum lift coefficients (fig. 17) increased almost linearly with increasing Reynolds number and obtained values of about 1.7 at R = 2.1×10^6 and about 2.1 at R = 9.0×10^6. The airfoil section exhibits a gradual type stall (fig. 6), particularly at the lower Reynolds numbers. Tuft pictures (not shown) and the pressure data of figure 11 indicated that the stall is of the turbulent or trailing-edge type.

The addition of a roughness strip at .075c (fig. 6) altered the lift characteristics because of changes in boundary-layer thickness, particularly at the lower test Reynolds numbers. For example, at R = 2.1×10^6 (fig. 6(a)) the angle of attack for zero lift coefficient changed from about -4.1° to -3.8°,

and the lift coefficient at $\alpha = 0°$ decreased from about 0.49 to 0.44. These effects on the lift characteristics decreased as the Reynolds number was increased and were essentially eliminated at $R = 9.4 \times 10^6$ (fig. 6(e)). Figure 13 shows that the roughness strip had only minor effects on the airfoil's maximum lift coefficients for the Reynolds number range tested. A comparison of the lift data obtained with a roughness strip (number 100 grit; sized for $R = 6.0 \times 10^6$) and with extensive roughness (no. 60 grit) wrapped around the leading-edge is shown in figure 7(a) for $R \approx 6.0 \times 10^6$. A decrease in the angle of attack for $c_{l,max}$ of about 5° and a decrease of about 19 percent in $c_{l,max}$ is shown for the wraparound roughness.

The effects of Mach number on the airfoil lift characteristics at a Reynolds number of $R \approx 6.0 \times 10^6$ are shown in figure 8(a) for the smooth airfoil and in figure 9(a) for the airfoil with a roughness strip located at $x/c = 0.075$. The expected Prandtl-Gauert increase in lift-curve slope is indicated by increasing the Mach number from 0.10 to 0.35. This same Mach number increase, however (figs. 8(a) and 9(a)) resulted in a decrease in the stall angle of attack of about 6° and about a 16 percent decrease in $c_{l,max}$. Figure 14 shows that most of this decrease in $c_{l,max}$ (about 12 percent) occurred above $M = 0.28$. These Mach number effects are a result of supercritical flow occurring near the leading-edge on the upper-surface of the airfoil.

Comparison of the data for the 17 percent GA(W)-1 and 13 percent GA(W)-2 airfoils for typical operating ranges of Reynolds numbers for light general aviation airplanes ($R = 2.0 \times 10^6$ to $R = 6.0 \times 10^6$) are shown in figures 10, 13 and 14. The predominant effect of decreasing the airfoil thickness is to increase the section lift coefficients in the high angle of attack range and

hence increase $c_{l,max}$ by about 0.10. Figure 13 shows that on the log scale the variation of $c_{l,max}$ with Reynolds number for the GA(W)-2 airfoil is almost a straight line and that the addition of a roughness strip had little effect. This contrasts with the S-type curve shown for the GA(W)-1 airfoil smooth and the decrease with the addition of roughness. This improvement in $c_{l,max}$ for the thinner airfoil is attributed to reduced upper-surface boundary-layer flow separation as illustrated by the pressure data comparison of figure 12(b). The effects of Mach number on $c_{l,max}$ for the two airfoils up to $M \approx 0.28$ are similar and are shown in figure 14 at $R \approx 6.0 \times 10^6$. Above $M = 0.28$ the GA(W)-2 airfoil indicates a large decrease in $c_{l,max}$. No data are available for the GA(W)-1 airfoil because of tunnel power limitations.

Comparisons of the maximum section lift coefficients of the GA(W)-2 airfoil with the older 12 percent NACA airfoils in a smooth condition are shown in figure 17. Increases in $c_{l,max}$ from about 0.20 to 0.40 throughout the Reynolds number range are indicated when compared to the 4 and 5 digit and 65 series. Thus, at a Reynolds number of 6.0×10^6, about a 24 percent improvement in $c_{l,max}$ is shown for the GA(W)-2 airfoil over the 4412 airfoil and a 16 percent improvement over the 23012 airfoil. Figure 18(a) shows a comparison of the lift characteristics of the NACA 4412, 23012, and 65_1-412 airfoils at a Reynolds number of 6.0×10^6 to the GA(W)-2 airfoil with extensive wrap-around roughness employed. Even for this extreme case of roughness the GA(W)-2 airfoil exhibited superior lift characteristics compared to the older NACA airfoils. Similar improvements in $c_{l,max}$ (fig. 19(a)) are shown compared to the recent data (ref. 7) obtained on a NACA 65_1-213 airfoil with the narrow strip roughness.

Comparison of the experimental lift data with the viscous flow theory of reference 8 for a Reynolds number of 3.0×10^6 and transition fixed at $x/c = 0.075$ are shown in figure 20. As previously reported (ref. 1), the theoretical method satisfactorily predicts the lift data for angles of attack where no significant boundary-layer flow separation is present.

Pitching-moment.- The pitching-moment coefficient data for the smooth airfoil (fig. 6) were generally insensitive to Reynolds number in the low angle of attack range and the addition of roughness only caused small positive increments in c_m. Comparison of the pitching-moment data for the Reynolds numbers tested show for angles of attack greater than about 6° and below the stall angle that the values of c_m are less negative at the low Reynolds numbers. This is typical of the decambering effect associated with boundary-layer thickening at the low Reynolds numbers. At a Reynolds number of about 6.0×10^6 increasing the Mach number from 0.10 to 0.35 (fig. 8(a)) caused no effect on the pitching-moment data up to about 8°. At the higher angles of attack a positive increment in c_m is shown.

Comparison of the data for the GA(W)-1 and GA(W)-2 airfoils in figure 10 show that the pitching-moment characteristics are essentially the same. Figure 18 (a) shows the expected more negative values of c_m for the GA(W)-2 airfoil, resulting from the aft camber for this type of airfoil, when compared to the older NACA airfoils. Comparisons of the experimental c_m data with the theory of reference 8 (fig. 20) indicate reasonable agreement only up to about $\alpha = 6°$.

Drag and lift-drag ratio.- The profile drag data of figure 6 indicate a "laminar bucket" in the drag polar for the smooth airfoil at the lower test Reynolds numbers. In practical general aviation application, no "laminar

bucket" would be expected because boundary-layer transition usually occurs near the leading edge of the airfoils, a result of roughness of construction or insect remains gathered in flight.

The addition of a roughness strip at .075c (fig. 6) resulted in essentially full chord turbulent flow which was confirmed by oil-flow techniques. The scale effects (fig. 15) at design lift-coefficient ($c_l = 0.40$) were generally consistent with flat-plate drag variations (ref. 6). Application of extensive wraparound roughness (fig. 7(b)) at $R \approx 6.0 \times 10^6$ indicates about 0.0010 increase in c_d at design lift, compared to the strip roughness, and large increases at higher lift coefficients. The drag data (fig. 9(b)) also indicate large increases in c_d at high lift coefficients by increasing the Mach numbers from 0.10 to 0.35.

Comparison of the drag data for the GA(W)-1 and GA(W)-2 airfoils for typical operating ranges of Reynolds numbers for light general aviation airplanes with fixed transition near the leading-edge are shown in figures 10, 15 and 16. Decreasing the airfoil thickness from 17 percent to 13 percent decreased the drag coefficient throughout the lift coefficient range (fig. 10) and extended the range of lift coefficients for low profile drag. At a typical cruise condition ($c_l = 0.40$, $R \approx 6.0 \times 10^6$) a decrease in c_d of about .0018 (fig. 15) is indicated by decreasing the airfoil thickness from 17 percent to 13 percent. This constitutes about a 22 percent increase in section lift-drag ratio. At a typical climb condition for light aircraft ($c_l = 1.0$, $R \approx 4.0 \times 10^6$) a decrease in c_d of about .0015 is shown. The corresponding values of lift-drag ratio (fig. 16) are about 77 (GA(W)-1) and 88 (GA(W)-2), or about a 14 percent improvement. The values of $(l/d)_{max}$ (fig. 10) vary from about 75 to 110 for Reynolds numbers of about 2.1×10^6 to 6.3×10^6 for the GA(W)-2

airfoil compared to about 65 to 90 for the GA(W)-1 airfoil. Also, the lift coefficient for maximum lift-drag ratio was increased by about 0.10 for the tninner airfoil.

Comparison of the drag data for the GA(W)-2 airfoil (wraparound roughness) with the NACA 4412, 23012, and 65_1-412 airfoils (fig. 18(b)) at a Reynolds number of about 6.0×10^6 with extensive wraparound roughness show about the same value of c_d at design lift coefficient ($c_l = 0.40$) for the GA(W)-2, 23012, and 4412 airfoils; however, the 65_1-412 airfoil indicates slightly lower values of c_d. The most noticable improvement resulting from the new airfoil design is the lower profile drag coefficients in the high lift coefficient range. This improvement is also shown (fig. 19(b)) when compared to the recent data (ref. 7) obtained with a narrow strip-roughness applied to the older NACA 65_1-213 airfoil.

SUMMARY OF RESULTS

The following results were determined from this investigation:

1. Maximum section lift coefficients at a Mach number of 0.15 increased from about 1.7 to 2.1 as the Reynolds number was increased from about 2.0×10^6 to 9.0×10^6.

2. Stall characteristics were generally gradual and of the trailing-edge type.

3. The application of a narrow roughness strip near the leading edge at a Reynolds number of about 6.0×10^6 resulted in small effects on lift, whereas extensive roughness wrapped around the leading edge resulted in a decrease in the maximum section lift coefficient of about 19 percent.

4. Increasing the Mach number from 0.10 to 0.35 at a constant Reynolds number of about 6.0×10^6 decreased the maximum section lift coefficient about

16 percent, with most of the decrease occurring above a Mach number of about 0.28.

5. The 13 percent GA(W)-2 airfoil compared to the 17 percent GA(W)-1 airfoil, provided about a 0.10 increase in maximum lift coefficient, reduced the profile drag coefficients at all lift coefficients, and increased the lift-drag ratio about 22 percent at cruise and about 14 percent at climb.

6. Maximum section lift coefficient at a Reynolds number of about 6.0×10^6 was about 16 percent greater than the older NACA 23012 airfoil section.

REFERENCES

1. McGhee, Robert J.; and Beasley, William D.: Low-Speed Aerodynamic Characteristics of a 17-Percent Thick Airfoil Section Designed for General Aviation Applications. NASA TN D-7428, 1973.

2. Pankhurst, R. C.; and Holder, D. W.: Wind Tunnel Technique. Sir Isaac Pitman and Sons Ltd., London, 1965.

3. Von Doenhoff, Albert E.; and Abbott, Frank T., Jr.: The Langley Two-Dimensional Low-Turbulence Pressure Tunnel. NACA TN 1283, 1947.

4. Braslow, Albert L.; and Knox, Eugene C.: Simplified Method for Determination of Critical Height of Distributed Roughness Particles for Boundary-Layer Transition at Mach Numbers from 0 to 5. NACA TN 4363, 1958.

5. Pope, Alan; and Harper, John J.: Low Speed Wind-Tunnel Testing. John Wiley and Sons, Inc., New York, 1966.

6. Abbott, Ira H.; and Von Doenhoff, Albert E.: Theory of Wing Sections, Dover Publications, Inc., New York, 1959.

7. Beasley, William D.; and McGhee, Robert J.: Experimental and Theoretical Low-Speed Aerodynamic Characteristics of the NACA 65_1-213, a = 0.50 Airfoil. NASA TM X-3160, 1975.

8. Stevens, W. A.; Goradia, S. H.; and Braden, J. A.: Mathematical Model For Two-Dimensional Multi-Component Airfoils in Viscous Flow. NASA CR-1843, 1971.

TABLE I.- NASA GA(w)-2 MEASURED AIRFOIL COORDINATES

[c = 61.01 cm (24.02 inches)]

x/c	$(z/c)_{upper}$	$(z/c)_{lower}$
0.0	0.0	0.0
.00199	.00922	-.00486
.00498	.01481	-.00847
.01246	.02365	-.01385
.02498	.03304	-.01870
.03747	.03957	-.02196
.04996	.04460	-.02465
.07494	.05230	-.02904
.09992	.05831	-.03246
.12490	.06323	-.03528
.14988	.06731	-.03769
.17485	.07080	-.03966
.19983	.07381	-.04129
.24980	.07857	-.04353
.29975	.08171	-.04471
.34971	.08357	-.04508
.39967	.08441	-.04475
.44963	.08425	-.04363
.49958	.08294	-.04149

x/c	$(z/c)_{upper}$	$(z/c)_{lower}$
.54954	.08025	-.03803
.57452	.07835	-.03582
.59950	.07609	-.03326
.62448	.07342	-.03048
.64946	.07035	-.02745
.67444	.06688	-.02428
.69942	.06305	-.02107
.72440	.05890	-.01783
.74938	.05446	-.01460
.77435	.04974	-.01145
.79933	.04476	-.00851
.82431	.03956	-.00587
.84929	.03417	-.00357
.87427	.02864	-.00187
.89925	.02296	-.00086
.92423	.01712	-.00052
.94921	.01112	-.00143
.97419	.00497	-.00377
.99917	-.00143	-.00720
1.0	-.00164	-.00732

TABLE II.- AIRFOIL ORIFICE LOCATIONS

c = 61.01 cm (24.02 inches)

Upper surface	Lower surface
x/c	x/c
0.00000	0.00000
.00630	.00672
.01288	.01309
.01945	.01840
.02667	.02427
.03790	.03819
.05259	.05080
.06353	.06424
.07630	.07805
.10133	.09993
.15209	.15314
.20155	.20053
.25083	.25038
.30067	.30131
.35354	.35046
.40190	.40252
.45097	.44832
.50103	.49918
.55120	.54706
.60165	.59871
.65170	.64990
.70128	.69962
.75175	.75038
.80139	.79851
.85013	.84896
.89997	.89990
.94943	.94981
.98925	.98800
	1.00 (base)

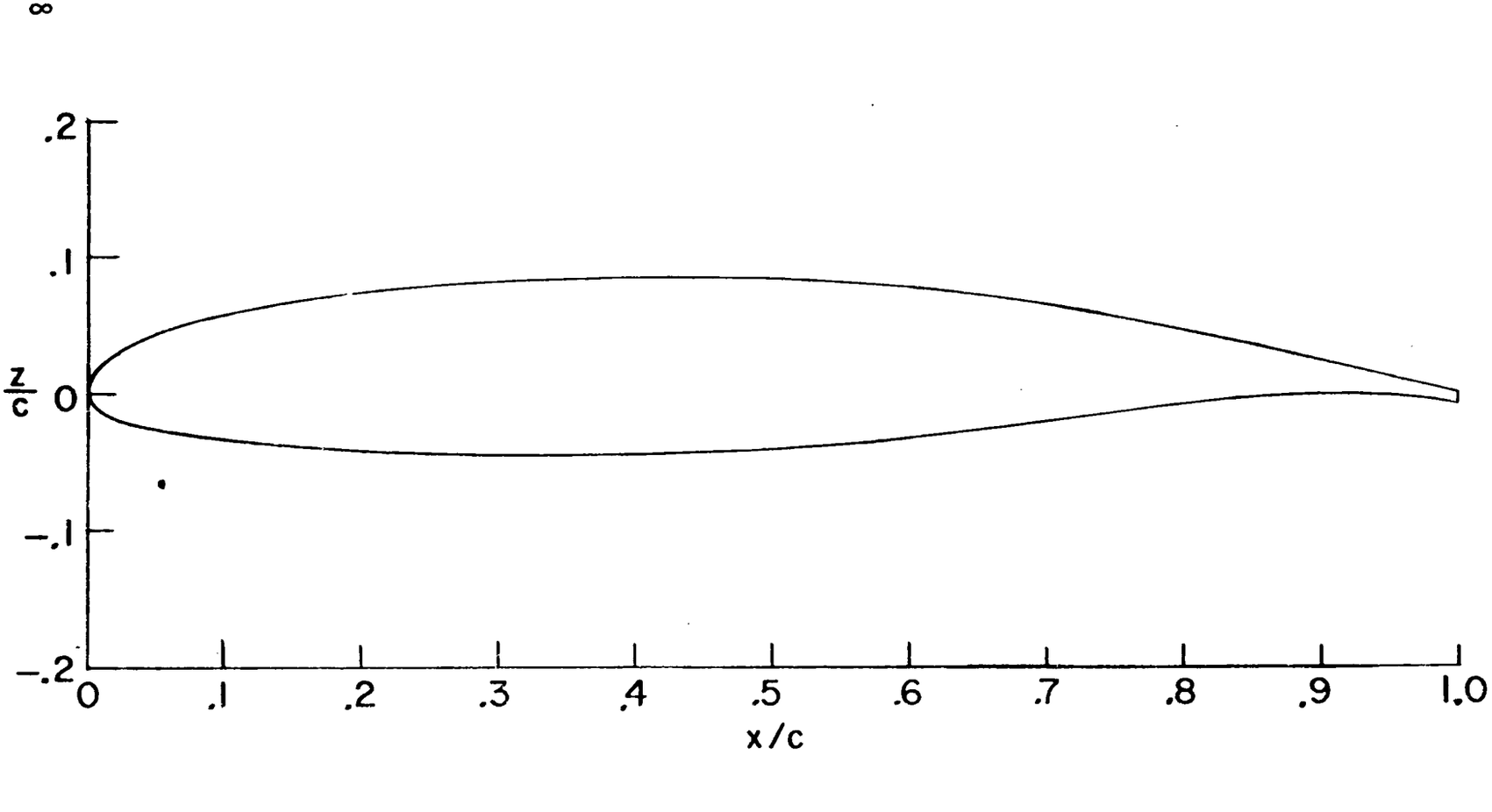

Figure 1.- Section shape for NASA GA(W)-2 airfoil.

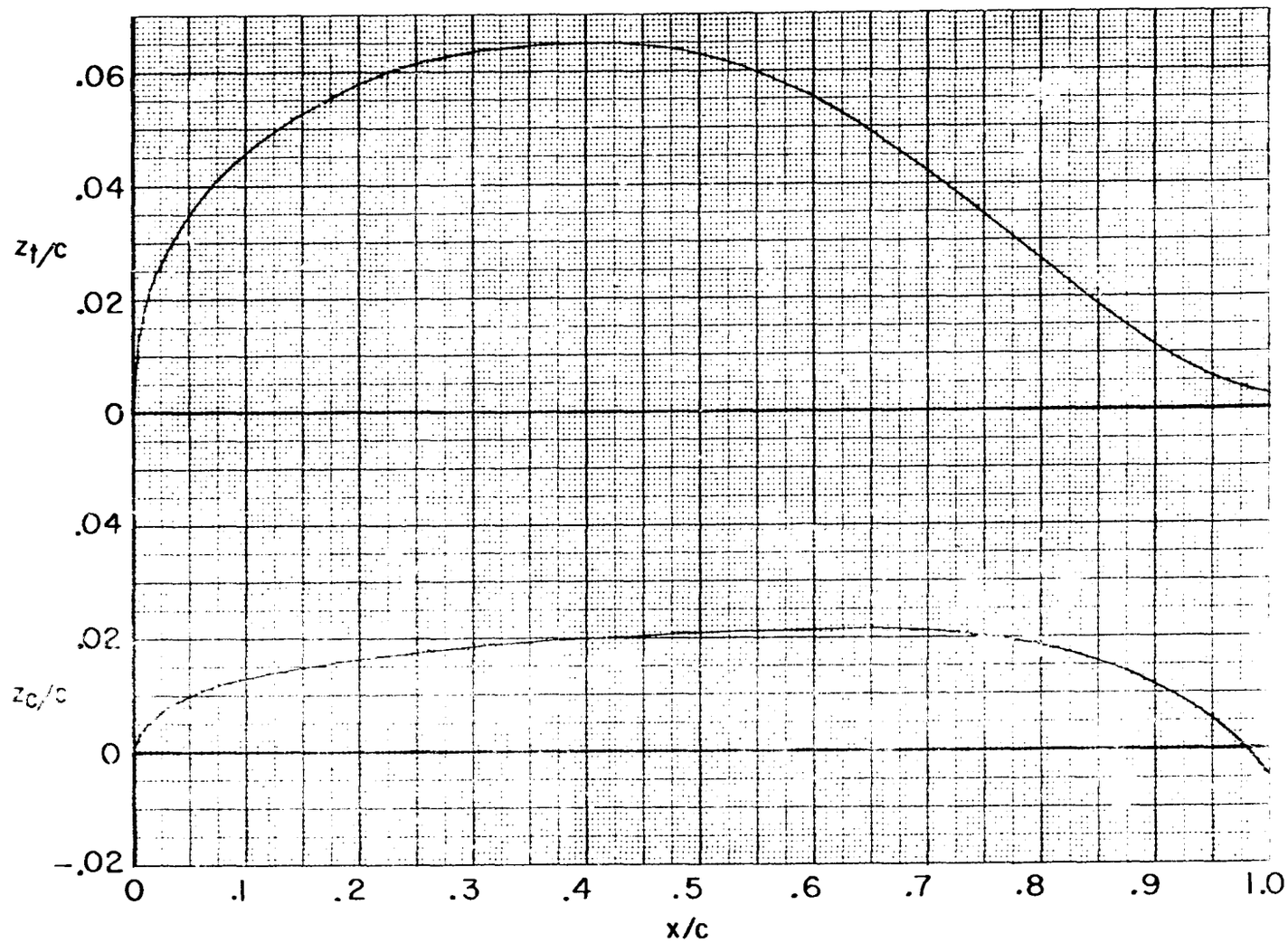

Figure 2.- Mean camber line and thickness distribution for NASA GA(W)-2 airfoil.

Figure 3. - Photograph of NASA GA(W)-2 airfoil.

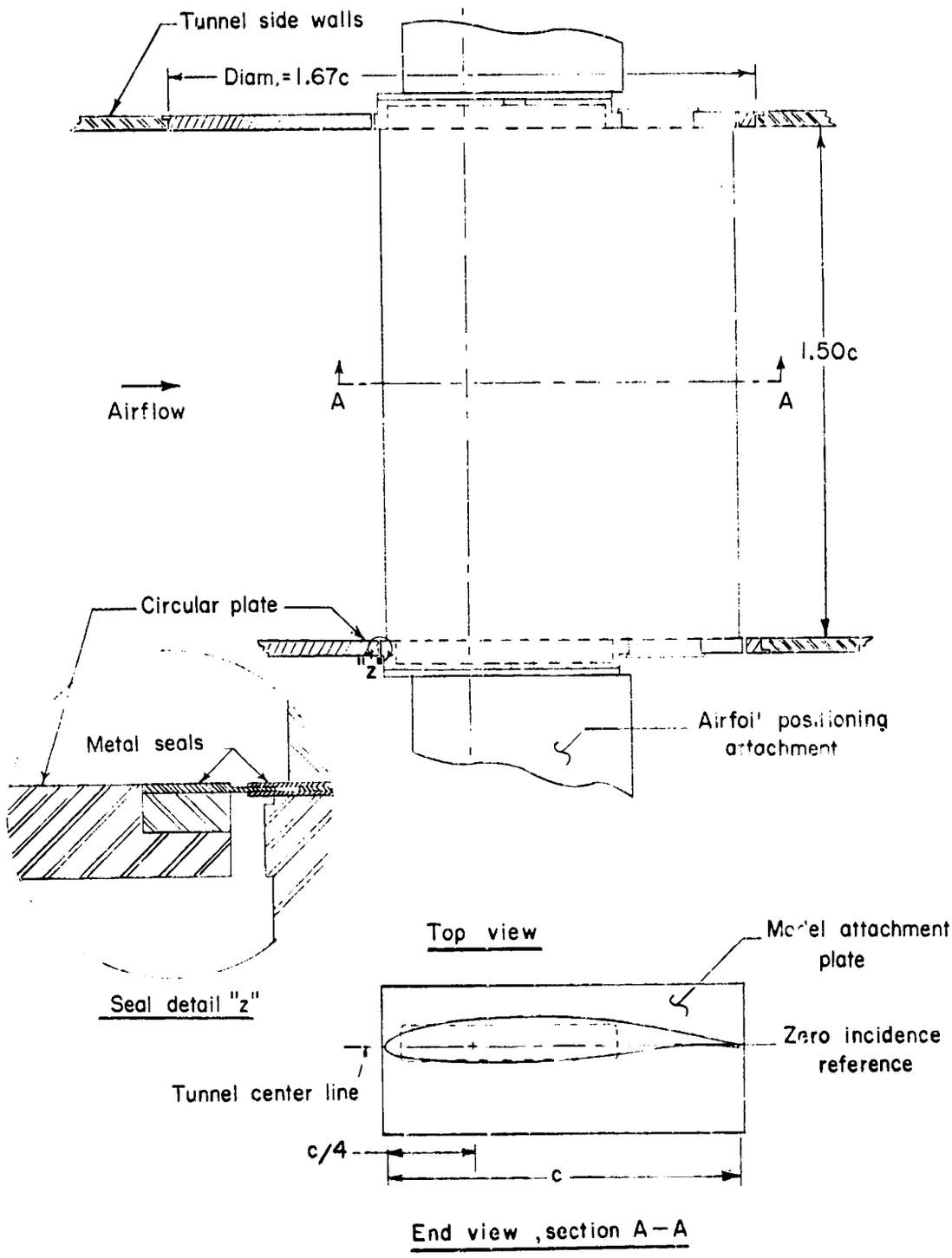

Figure 4.- Airfoil mounted in wind-tunnel. All dimensions in terms of airfoil chord. c = 61.01 cm (24.02 in.).

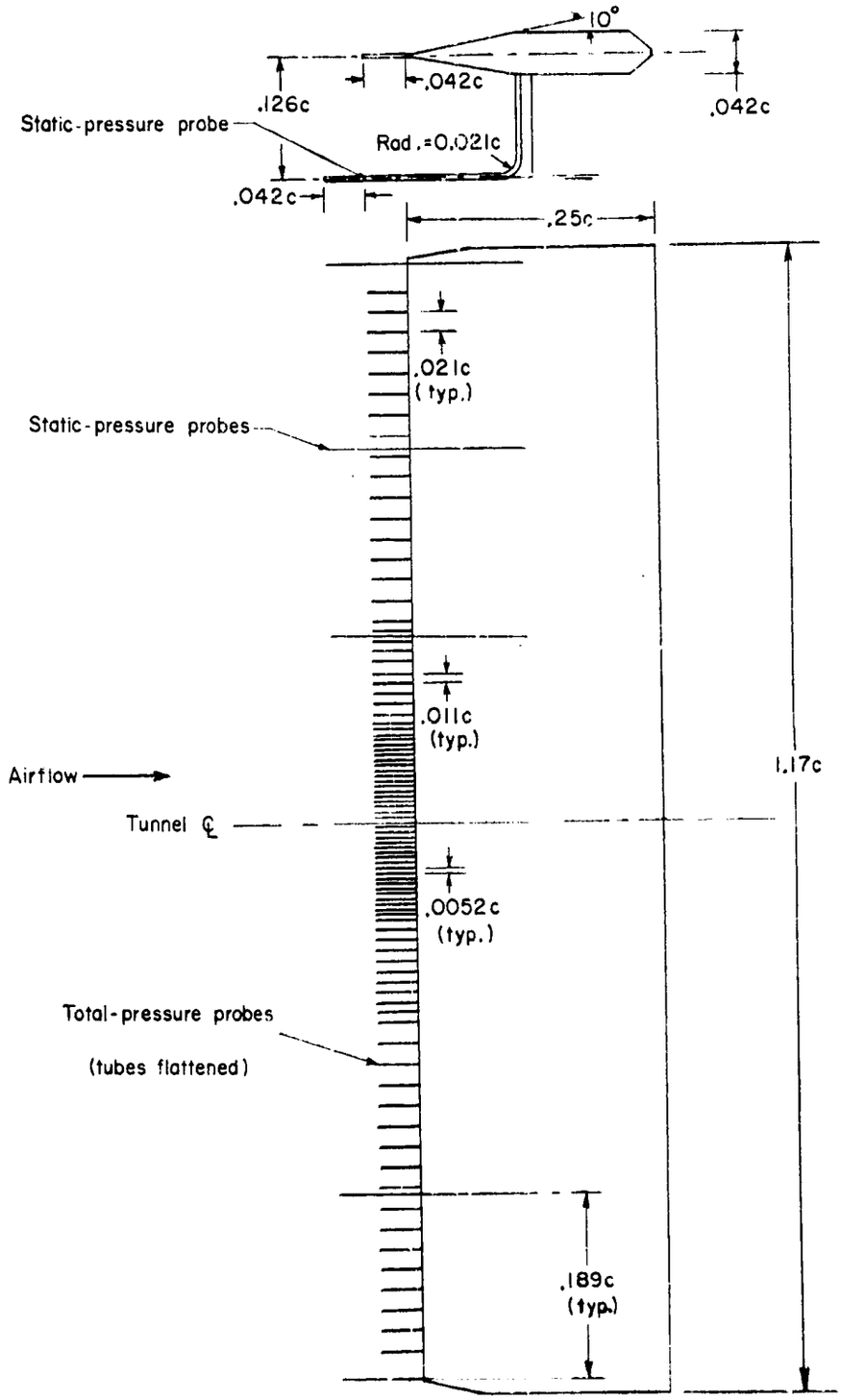

Figure 5.- Drawing of wake rake. All dimensions in terms of airfoil chord. c = 61.01 cm (24.02 in.).

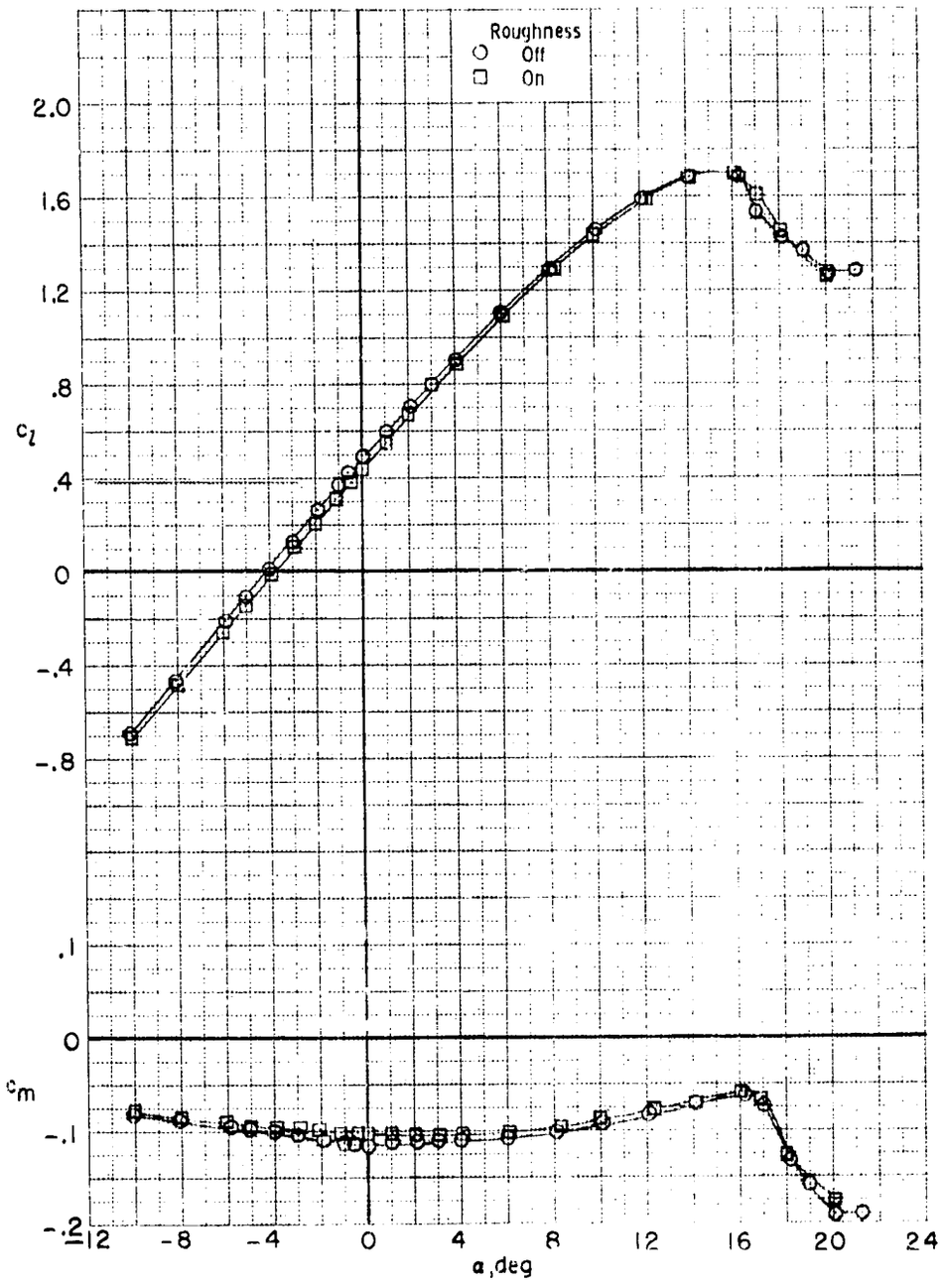

(a) $R = 2.1 \times 10^6$.

Figure 6.- Effect of Reynolds number on airfoil section characteristics. $M = 0.15$.

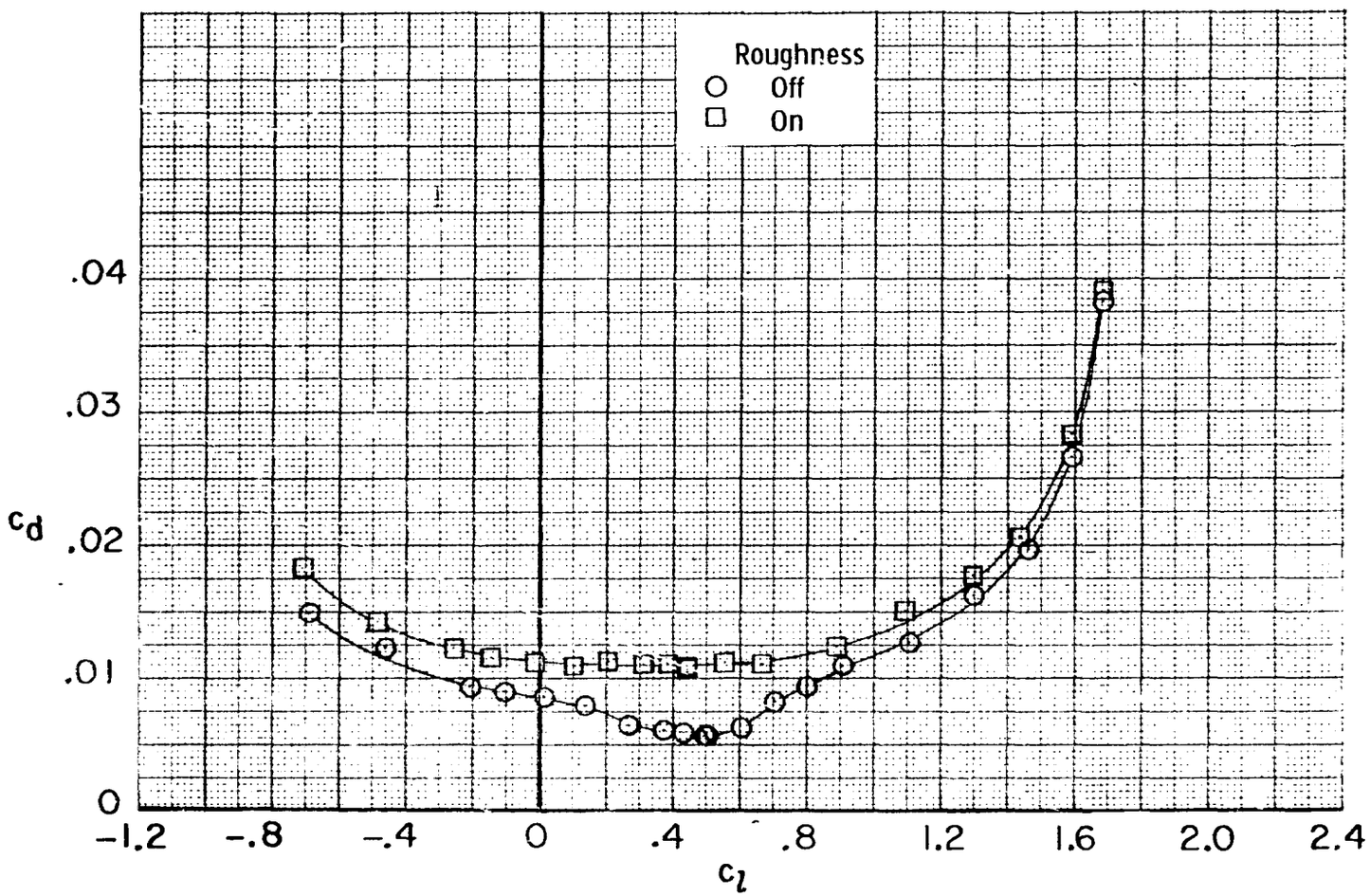

(a) R = 2.1 x 10^6. Concluded.

Figure 6.- Continued.

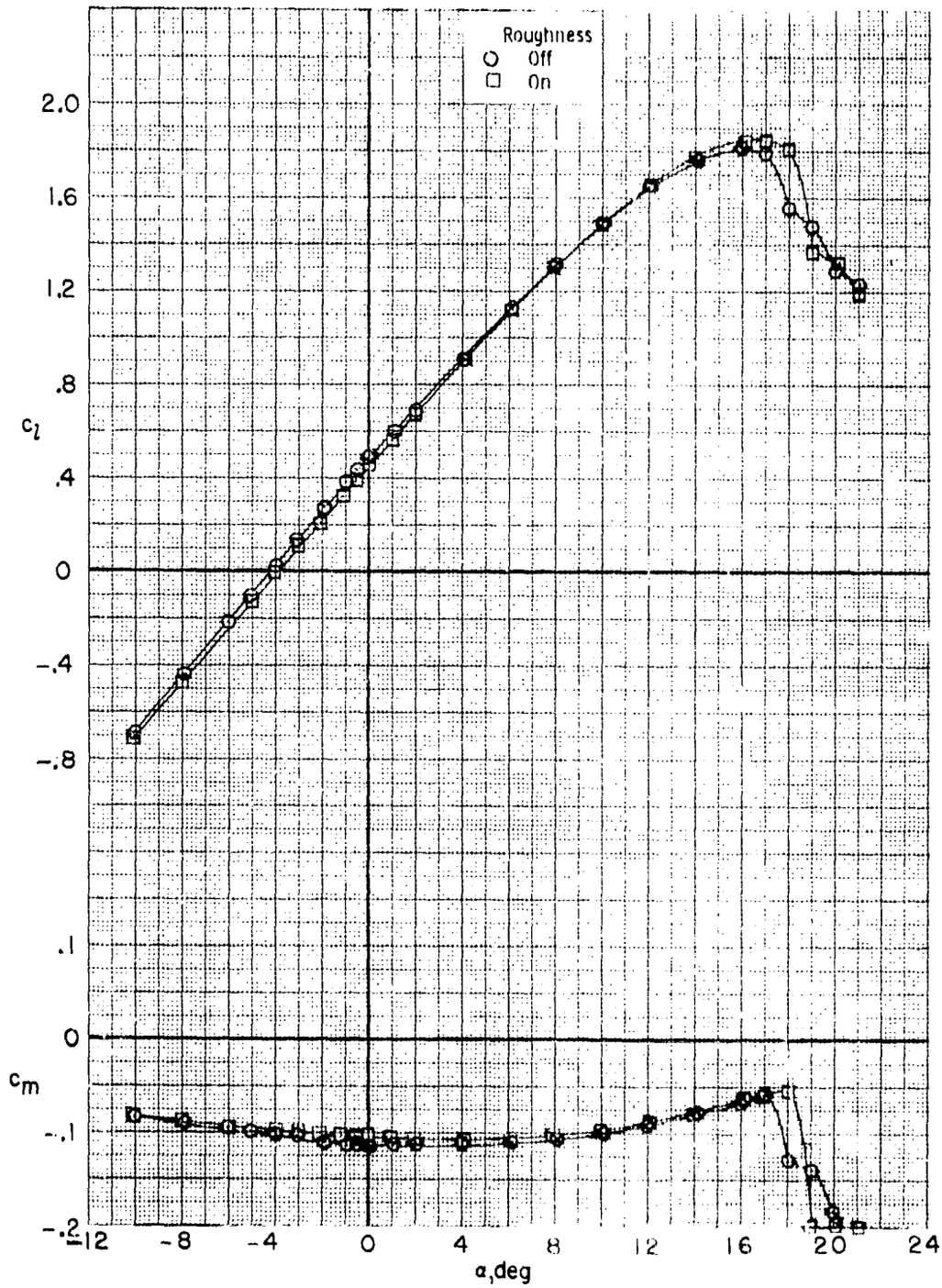

(b) $R = 3.2 \times 10^6$.

Figure 6.- Continued.

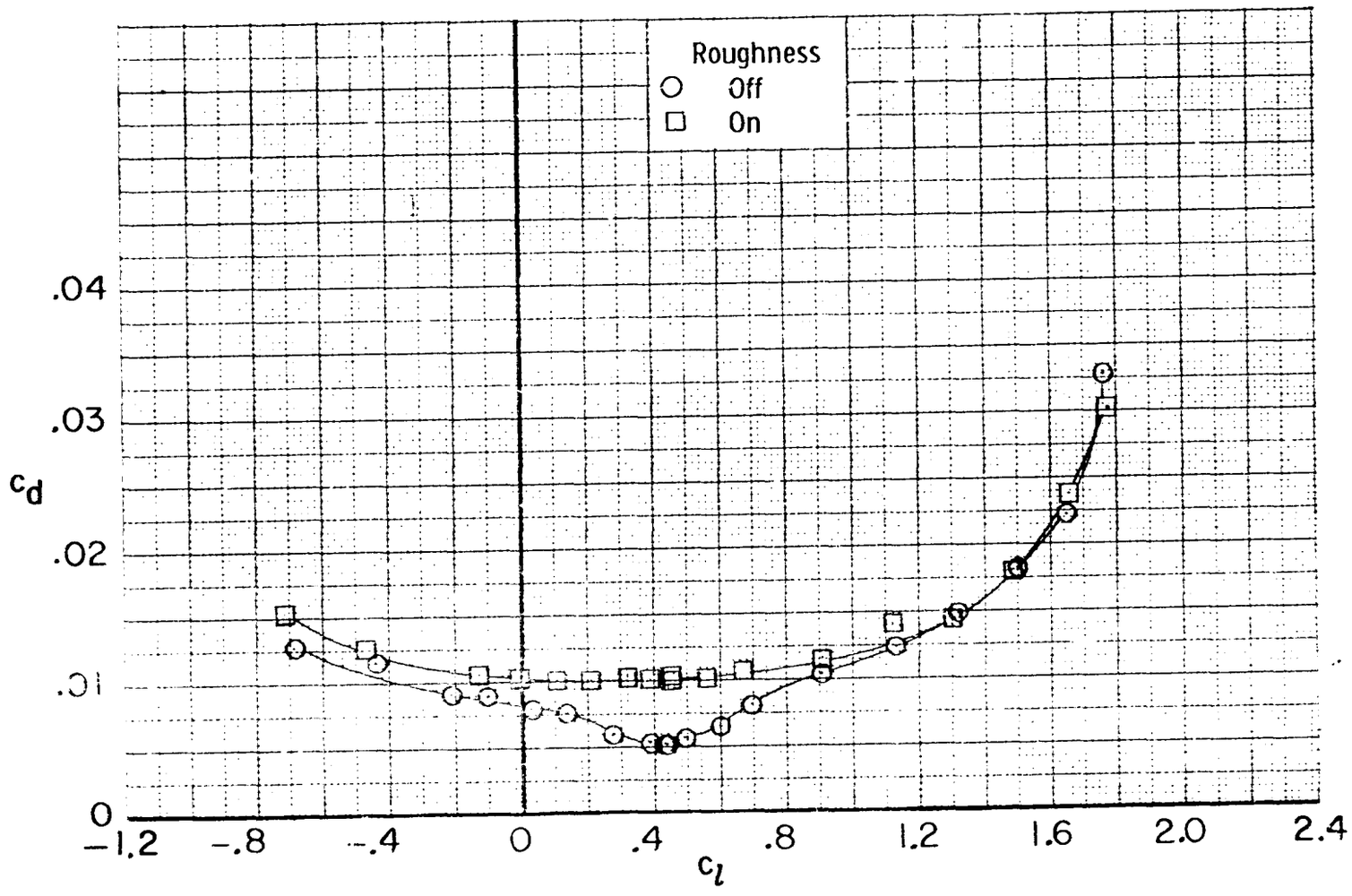

(b) $R = 3.2 \times 10^6$. Concluded.

Figure 6.- Continued.

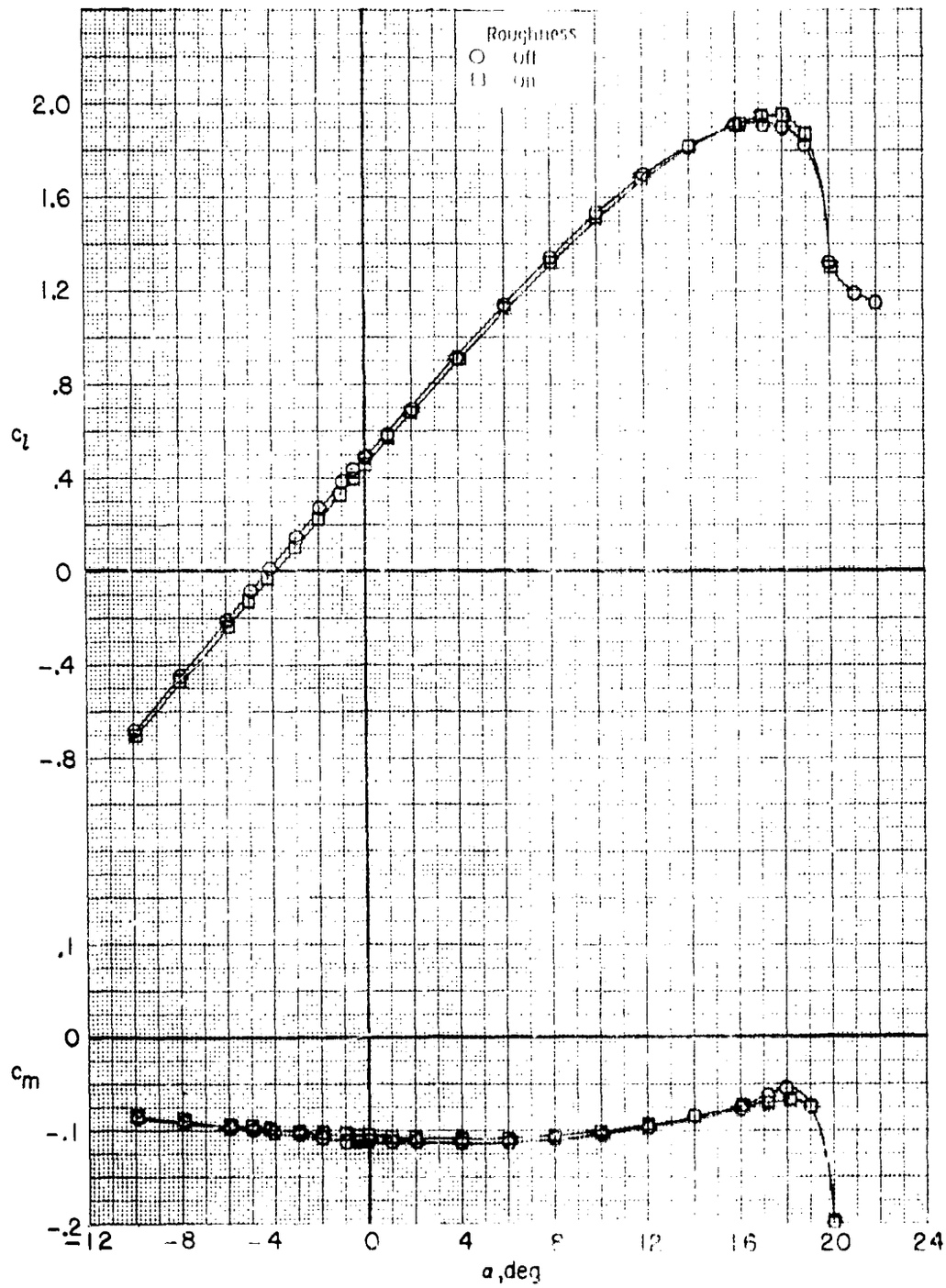

(c) $R = 4.1 \times 10^6$.

Figure 6.– Continued.

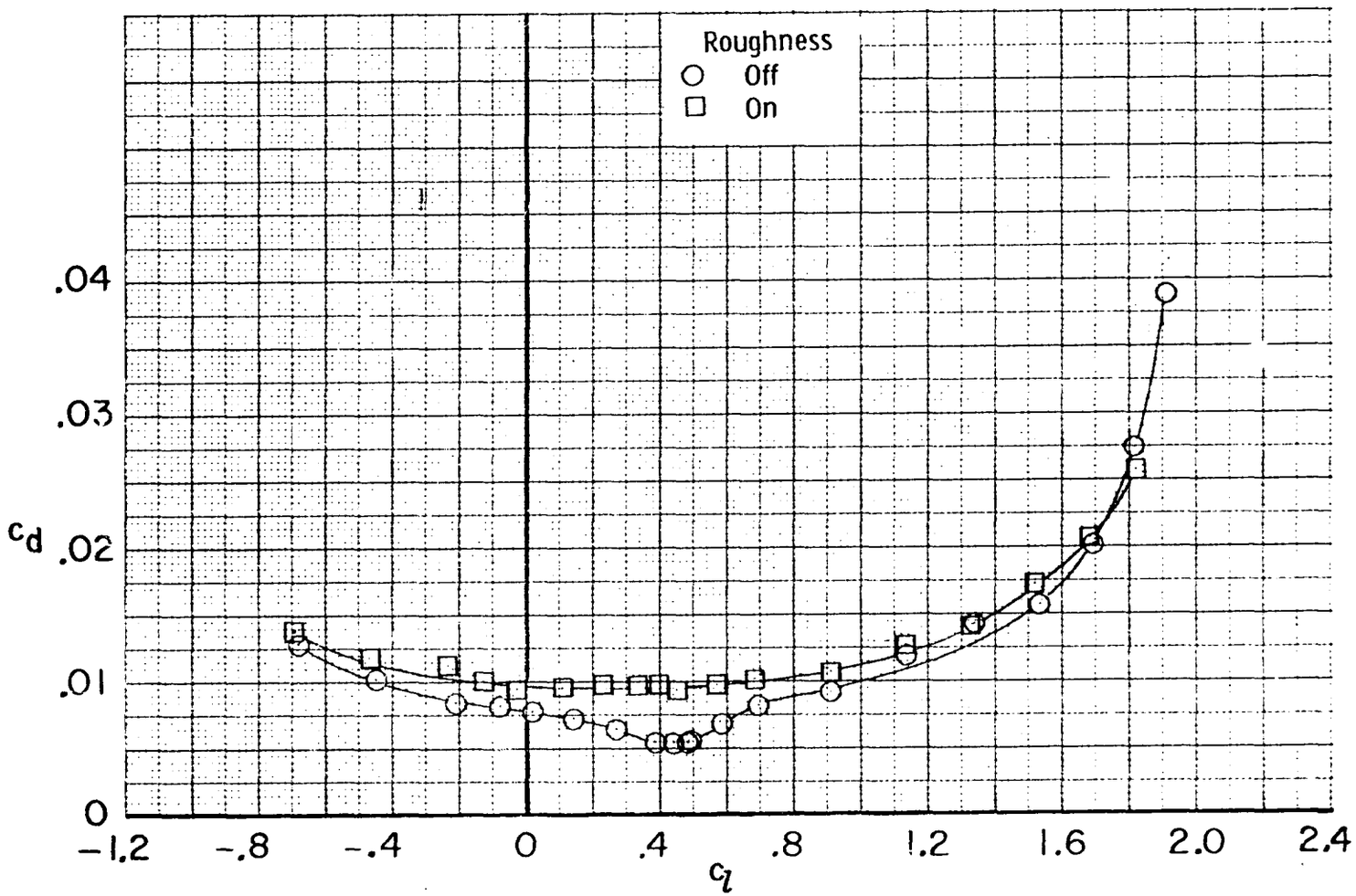

(c) R = 4.1 x 10^6. Concluded.

Figure 6.- Continued.

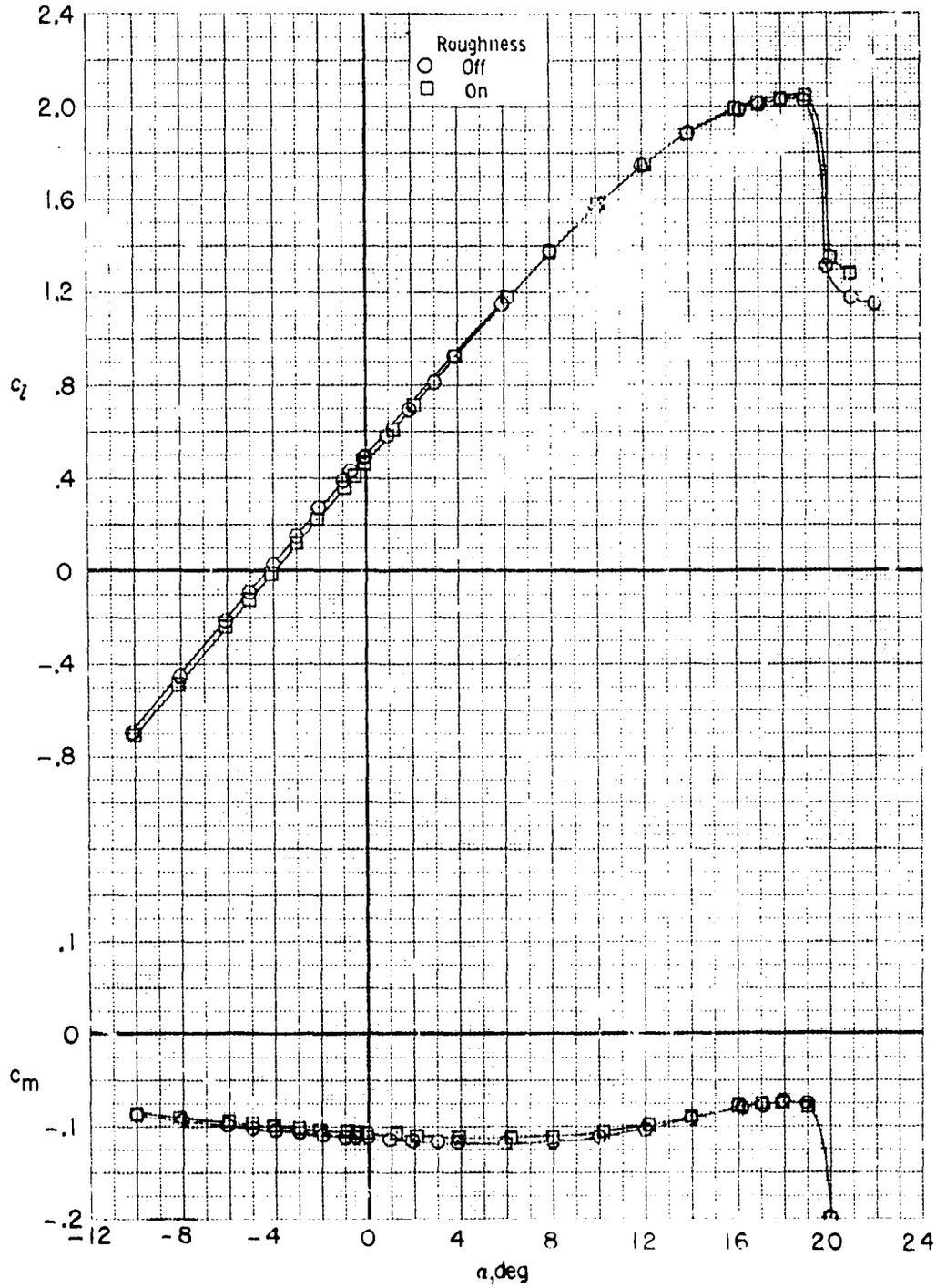

(d) $R = 6.1 \times 10^6$.

Figure 6.- Continued.

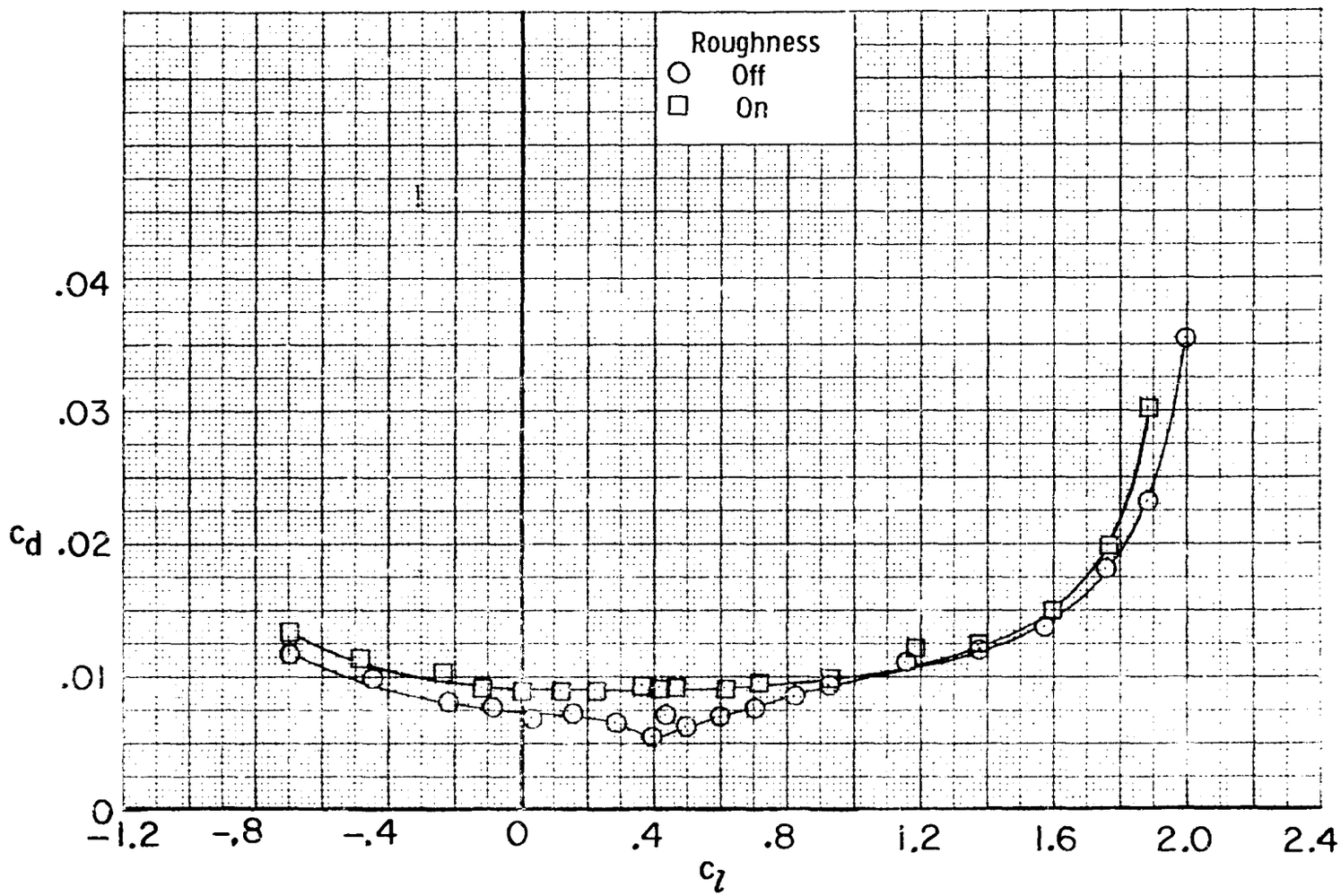

(d) R = 6.1 x 10^6. Concluded.

Figure 6. - Continued.

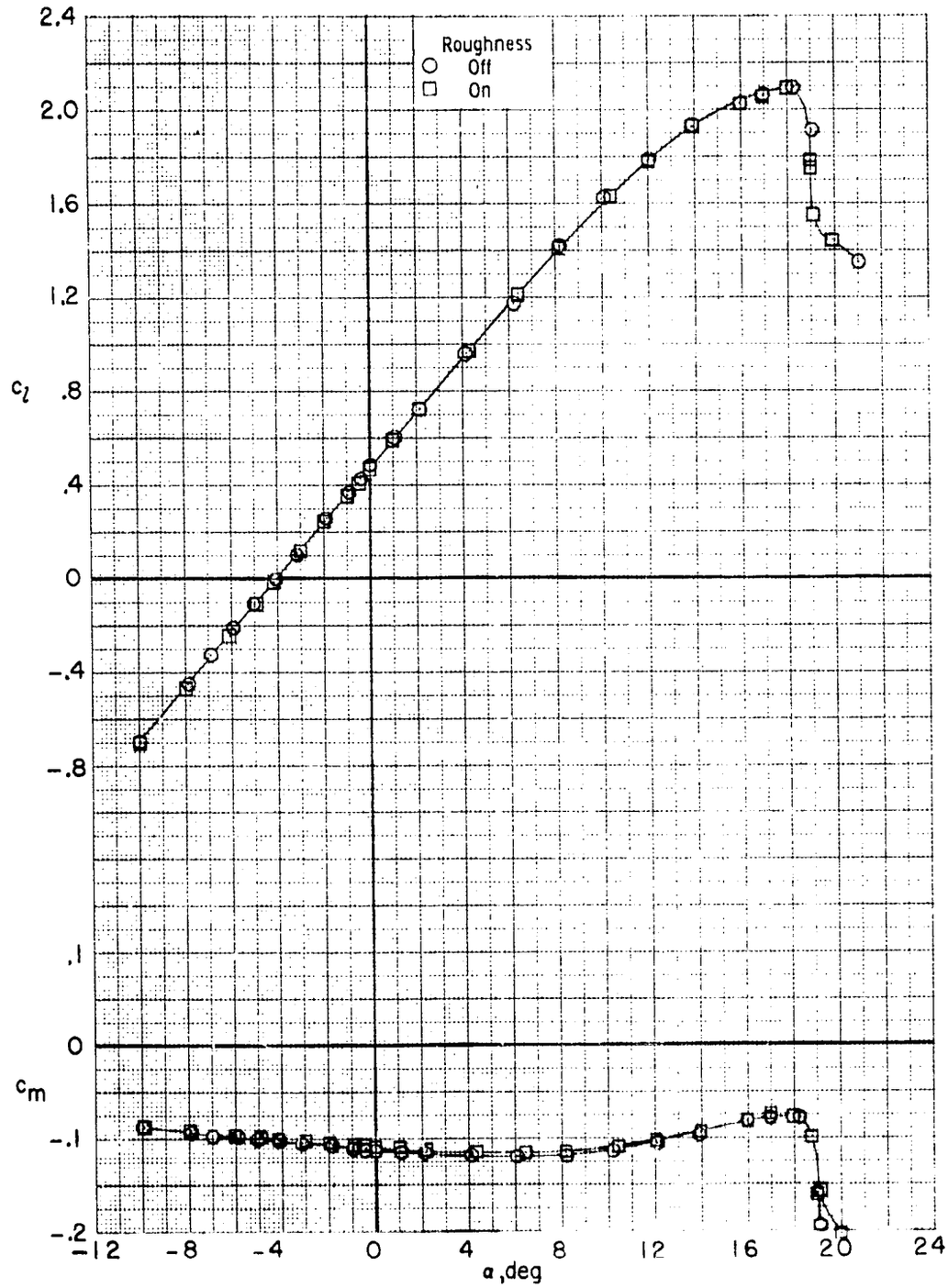

(e) $R = 9.4 \times 10^6$.

Figure 6.- Continued.

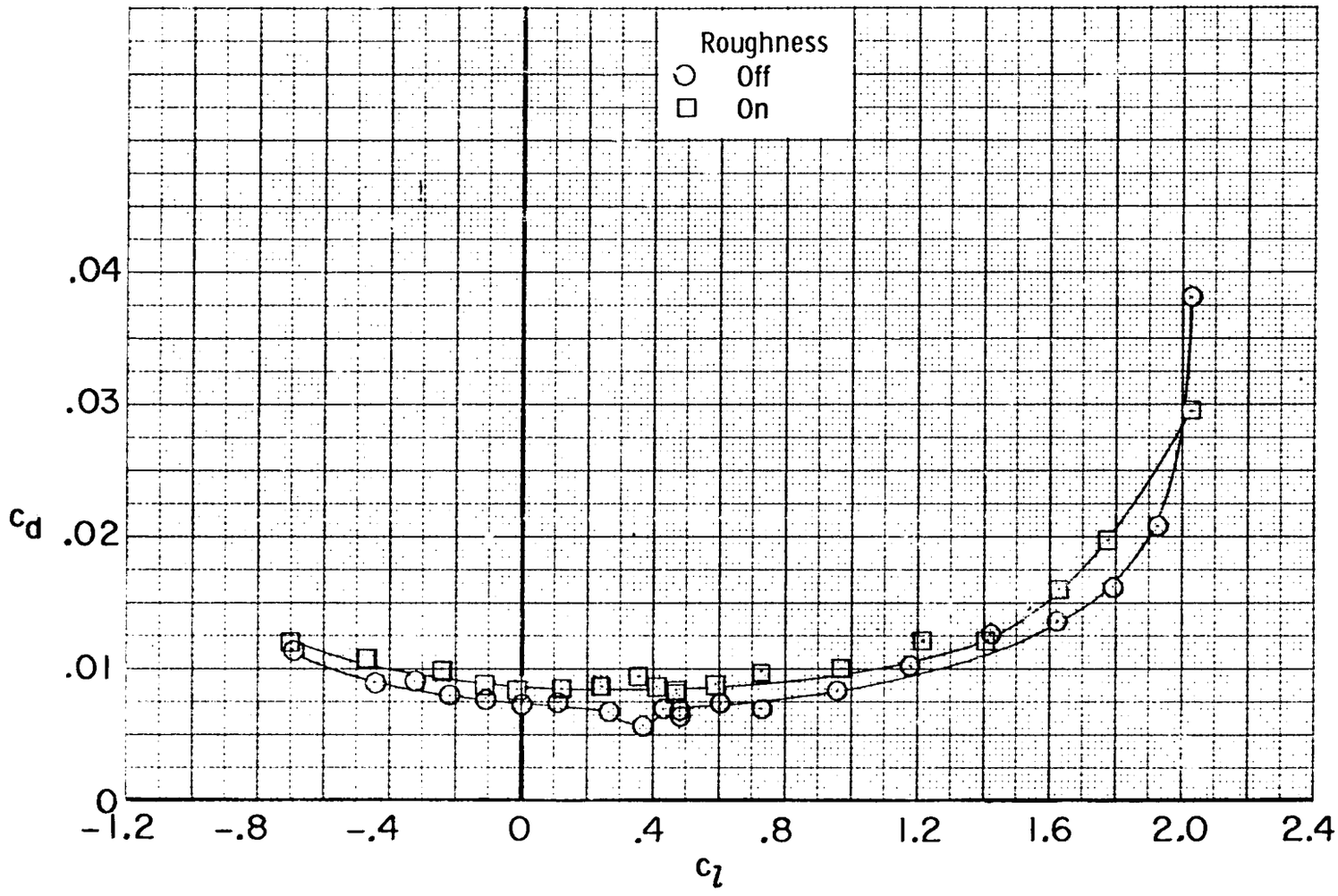

(e) R = 9.4 x 10^6. Concluded.

Figure 6.- Concluded.

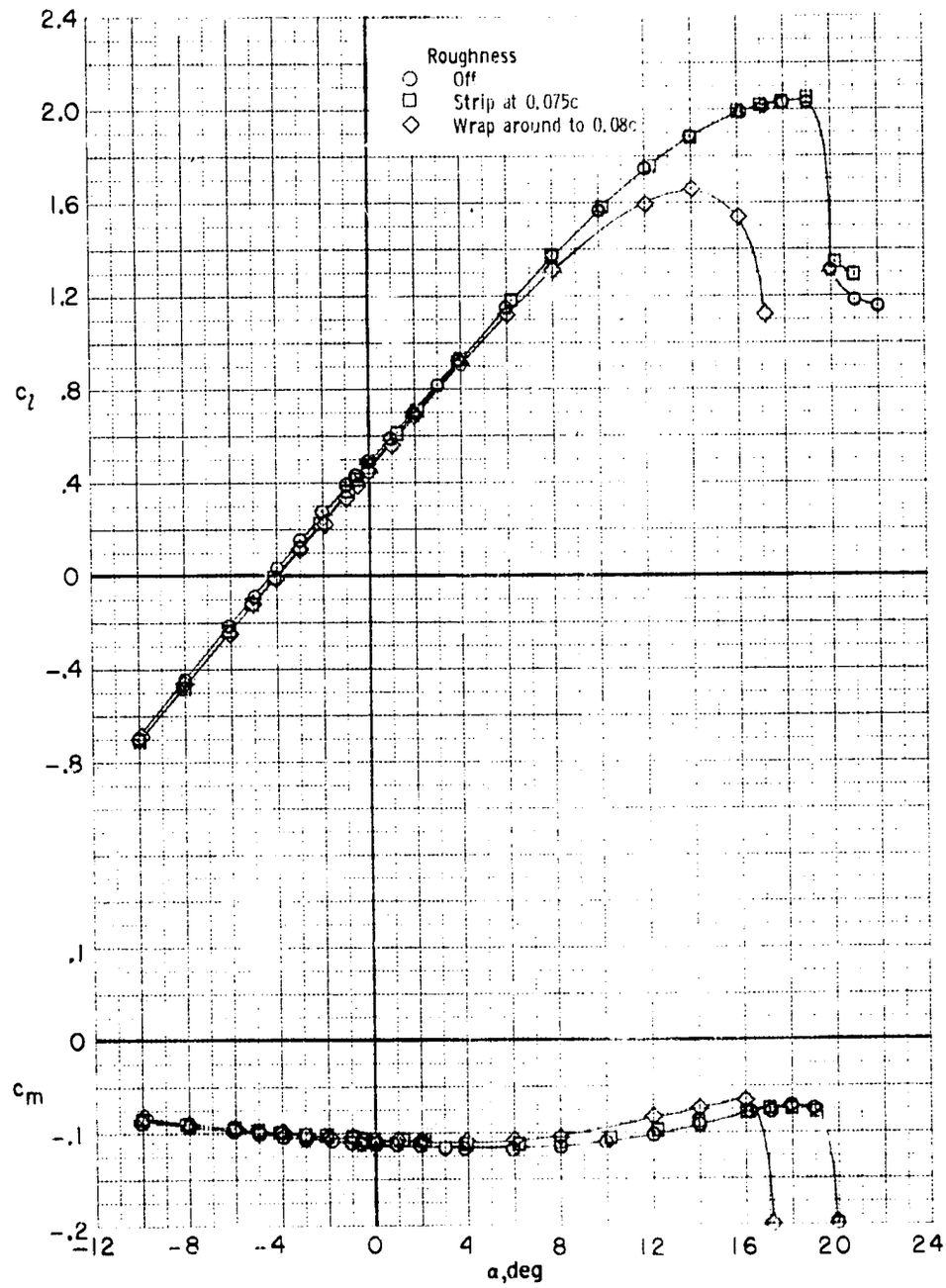

(a) Lift and moment data.

Figure 7.- Effect of roughness configuration on airfoil section characteristics.

$M = 0.15$; $R \approx 6.0 \times 10^6$.

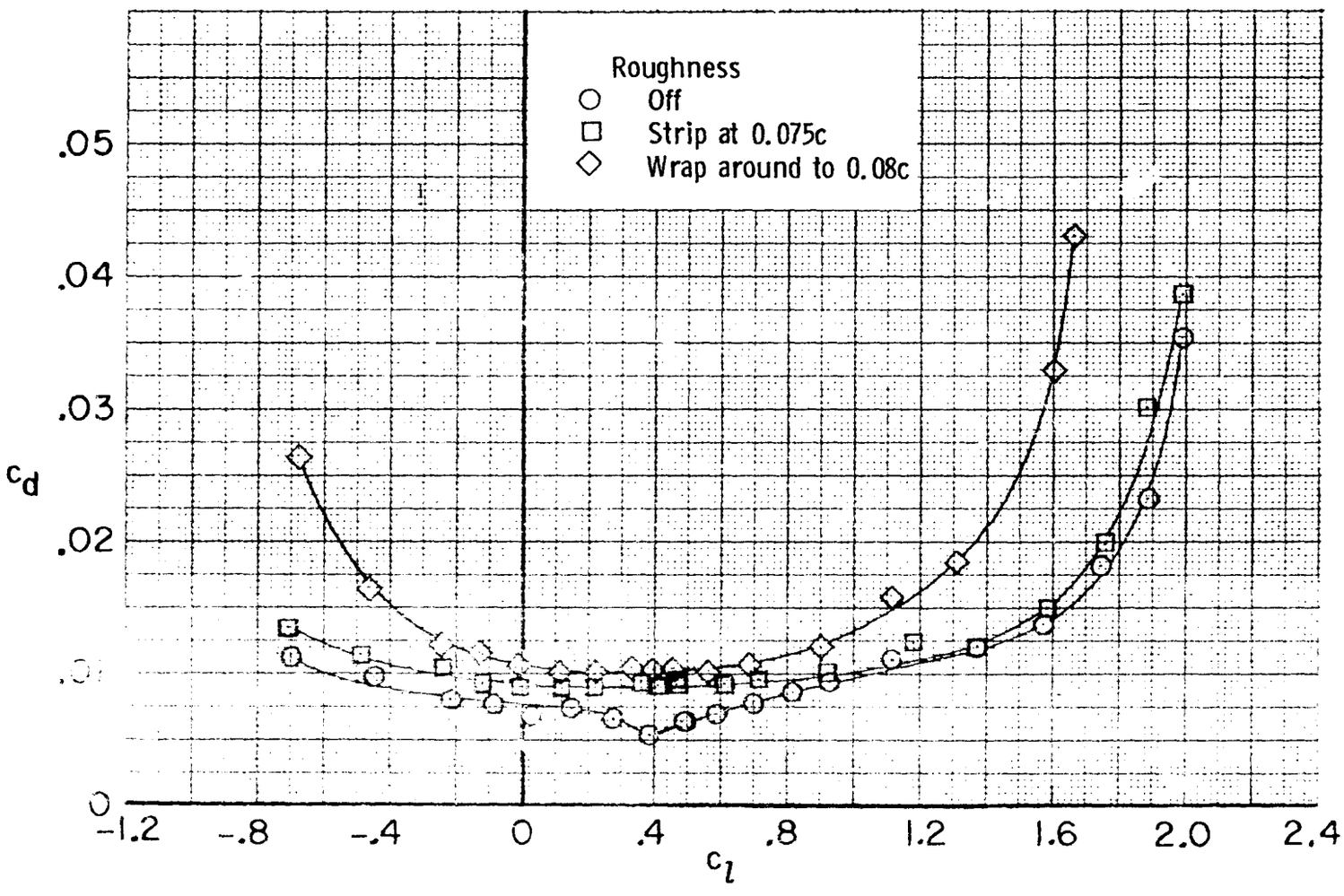

(b) Drag polars.

Figure 7.- Concluded.

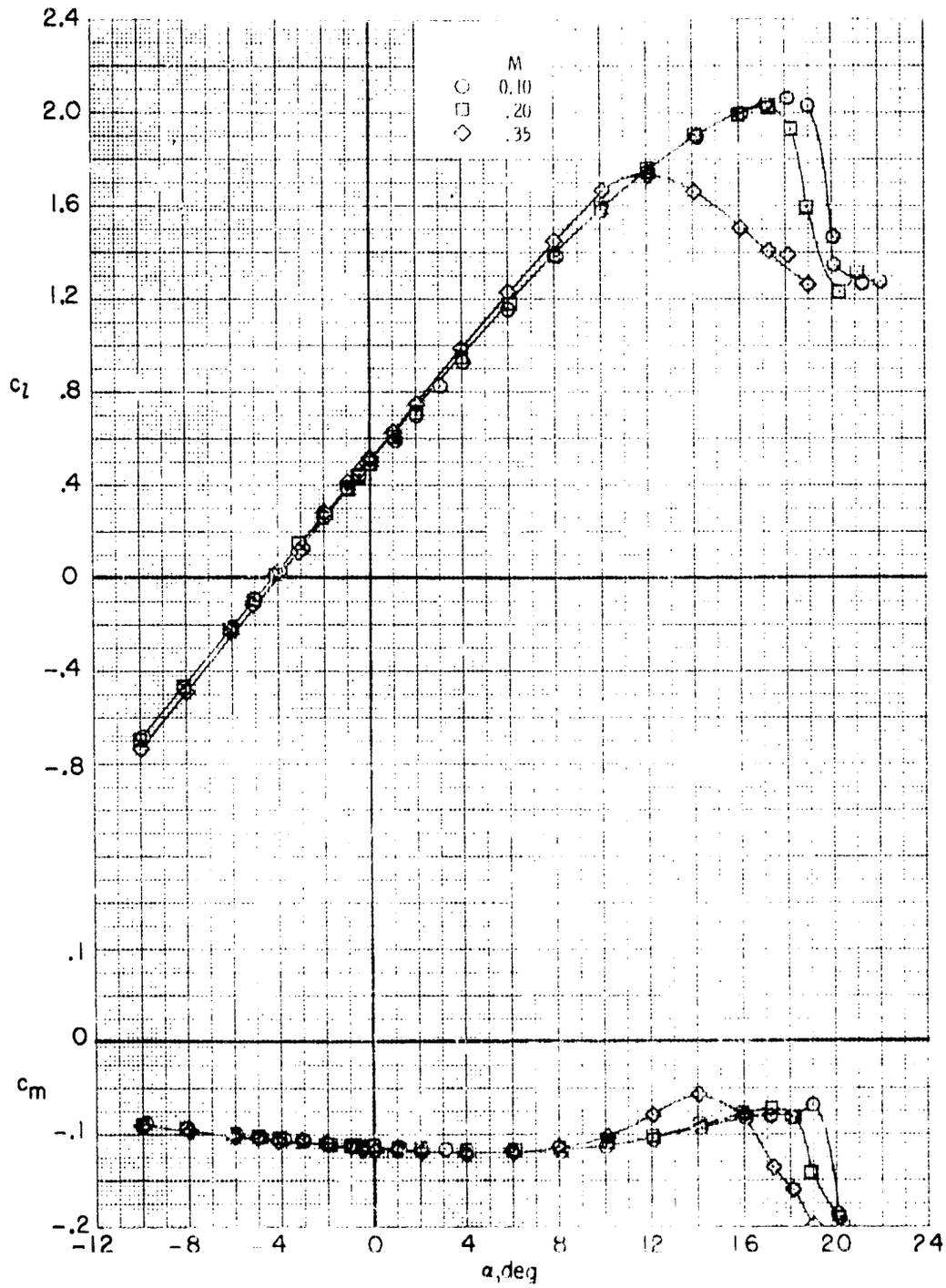

(a) Lift and moment data.

Figure 8.- Effect of Mach number on airfoil section characteristics. $R \approx 6.0 \times 10^6$; smooth airfoil.

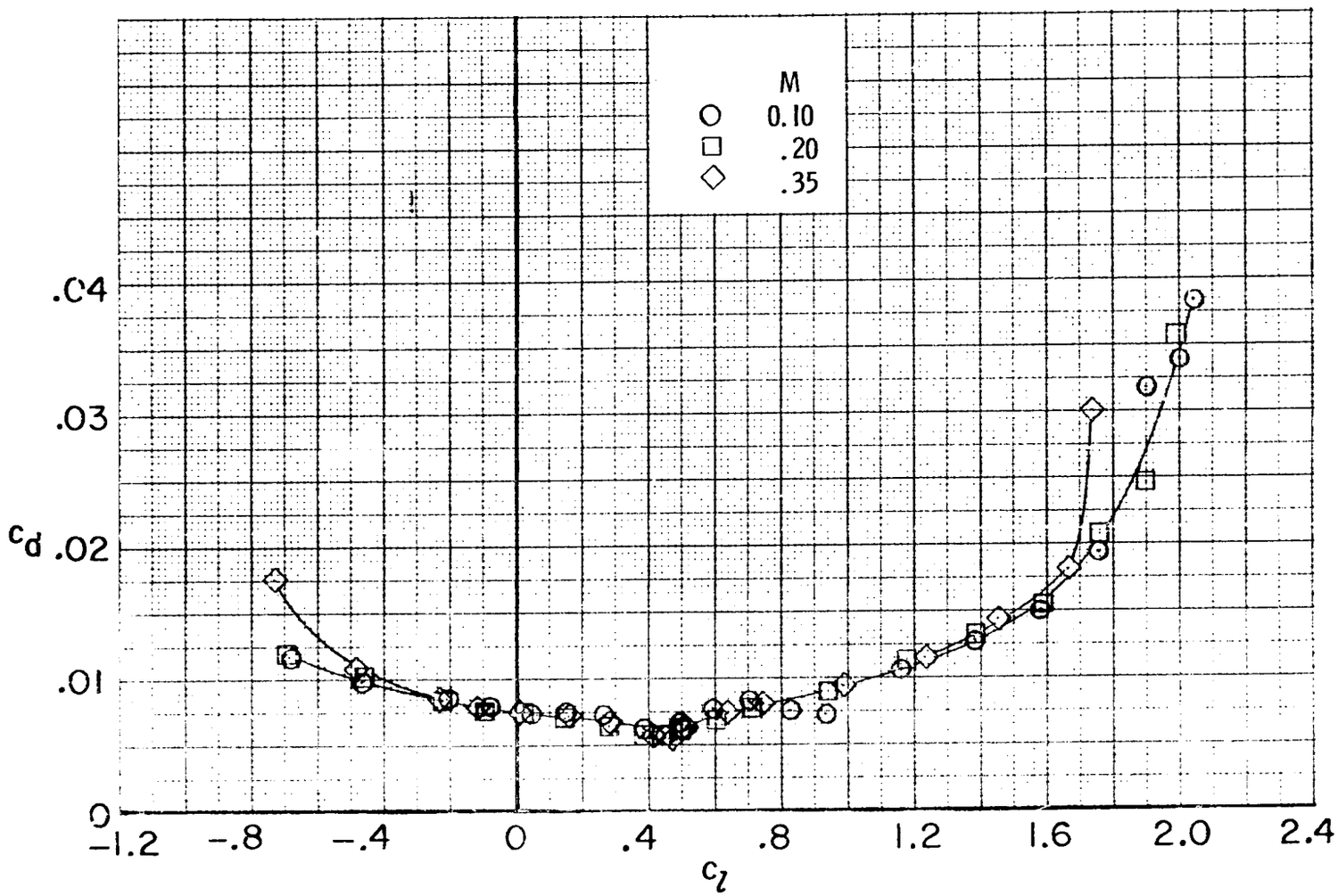

(b) Drag polars.

Figure 8.- Concluded.

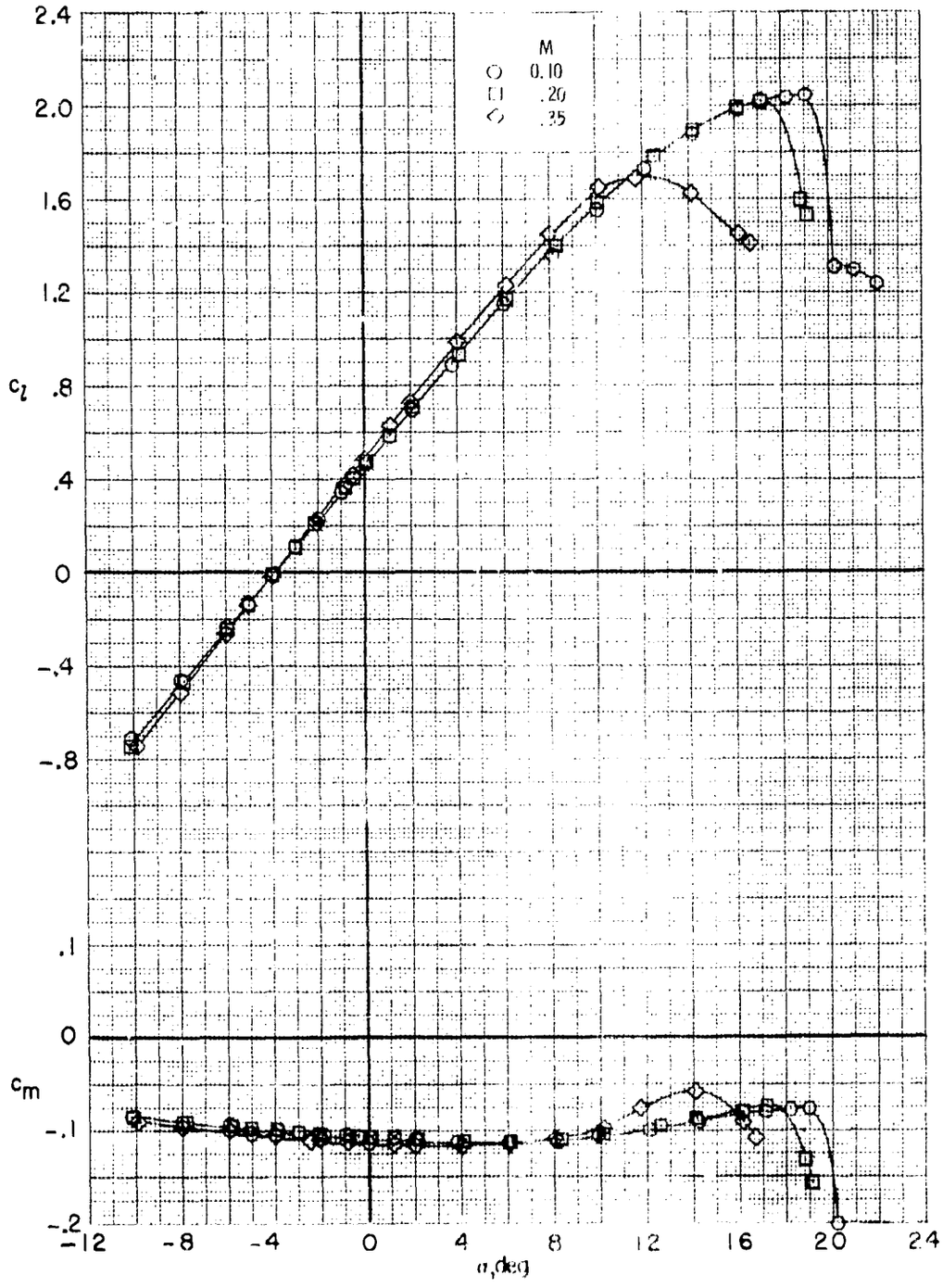

(a) Lift and moment data.

Figure 9.- Effect of Mach number on airfoil section characteristics.

$R \approx 6.0 \times 10^6$; transition fixed at $x/c = 0.075$.

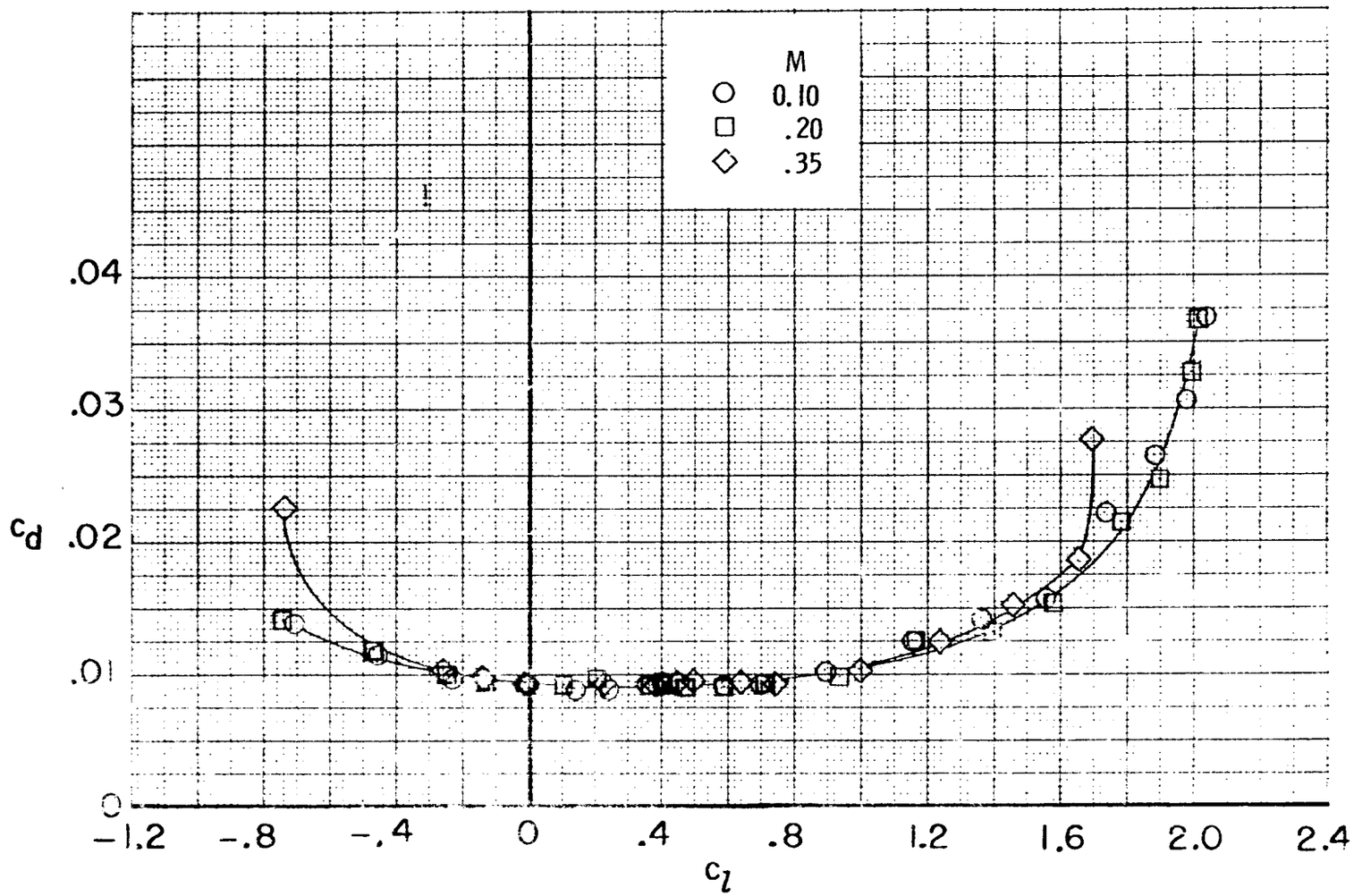

(b) Drag polars.

Figure 9.- Concluded.

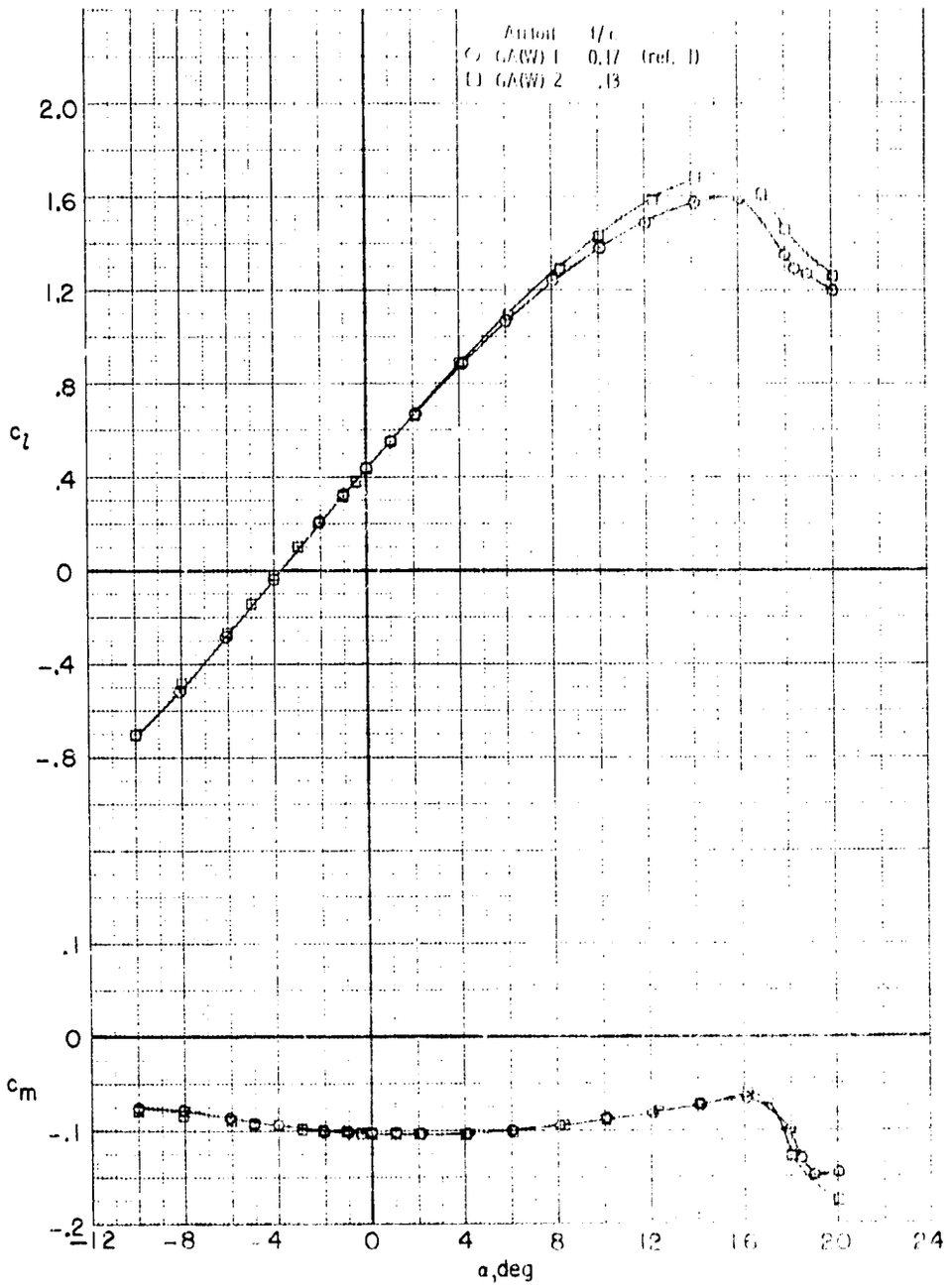

(a) $R = 2.1 \times 10^6$.

Figure 10.- Comparison of the section characteristics for the GA(W)-1 and GA(W)-2 airfoils. M = 0.15; transition fixed at x/c = 0.075.

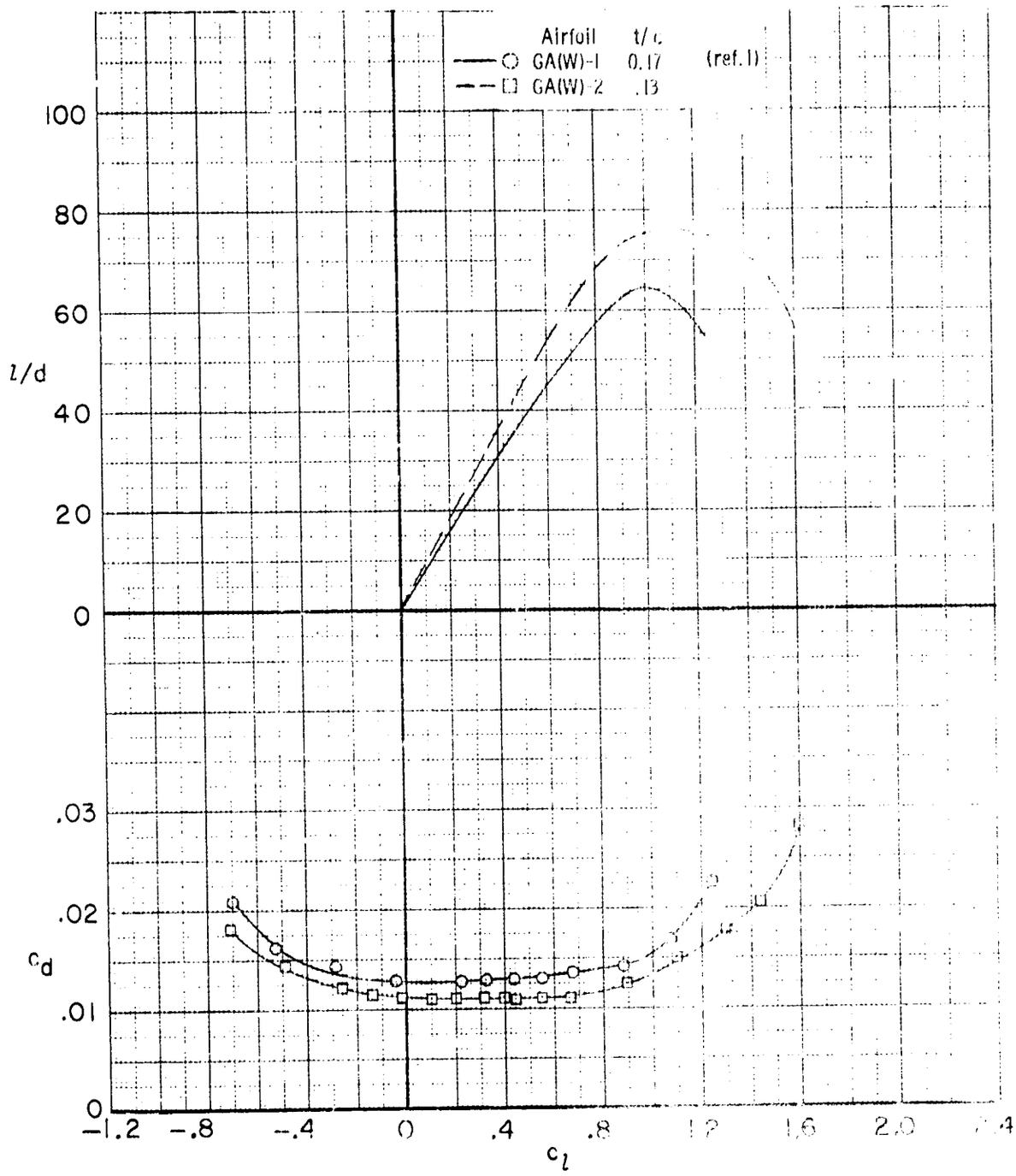

(a) $R = 2.1 \times 10^6$. Concluded.

Figure 10. - Continued.

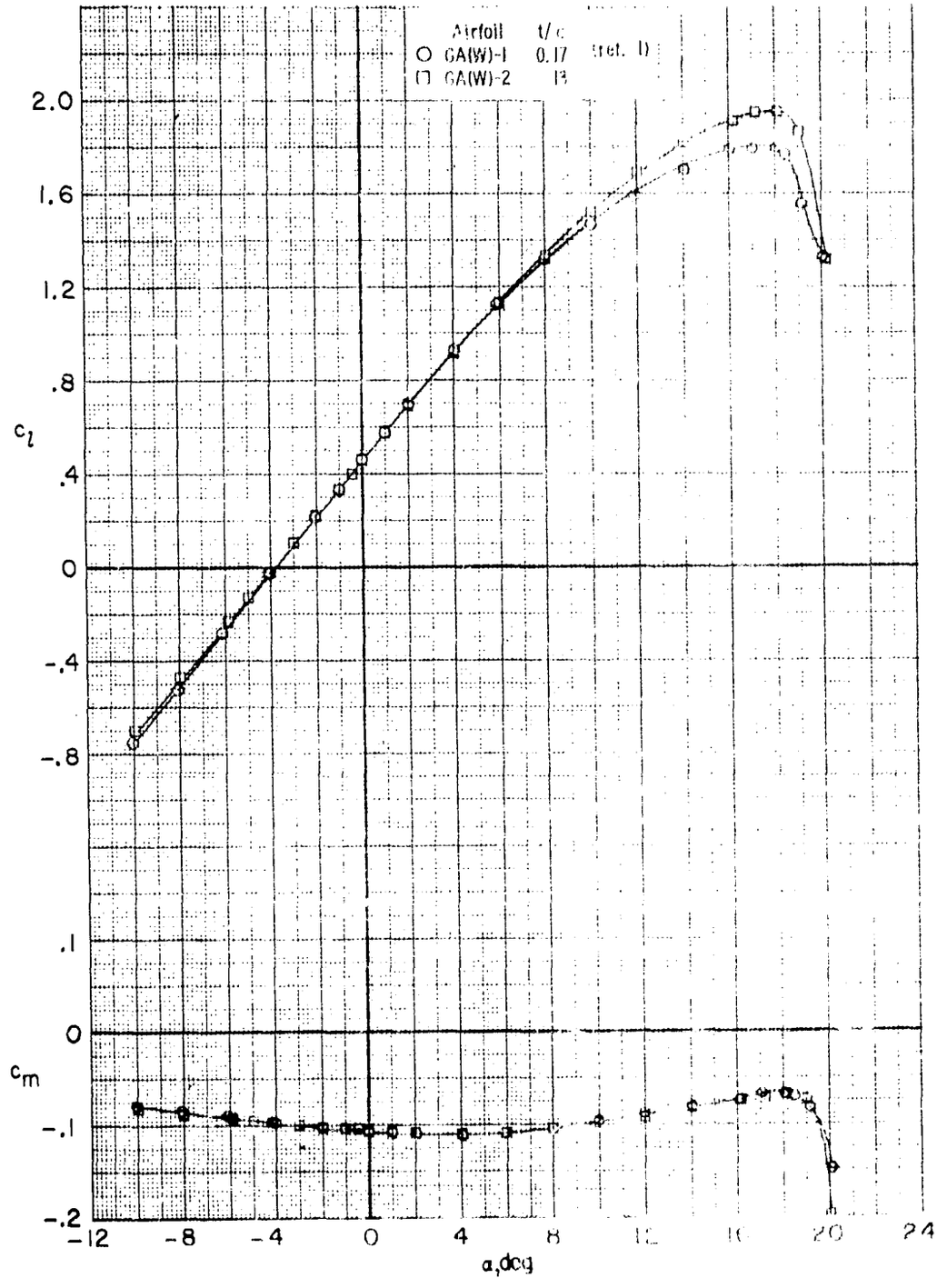

(b) $R = 4.3 \times 10^6$.

Figure 10.- Continued.

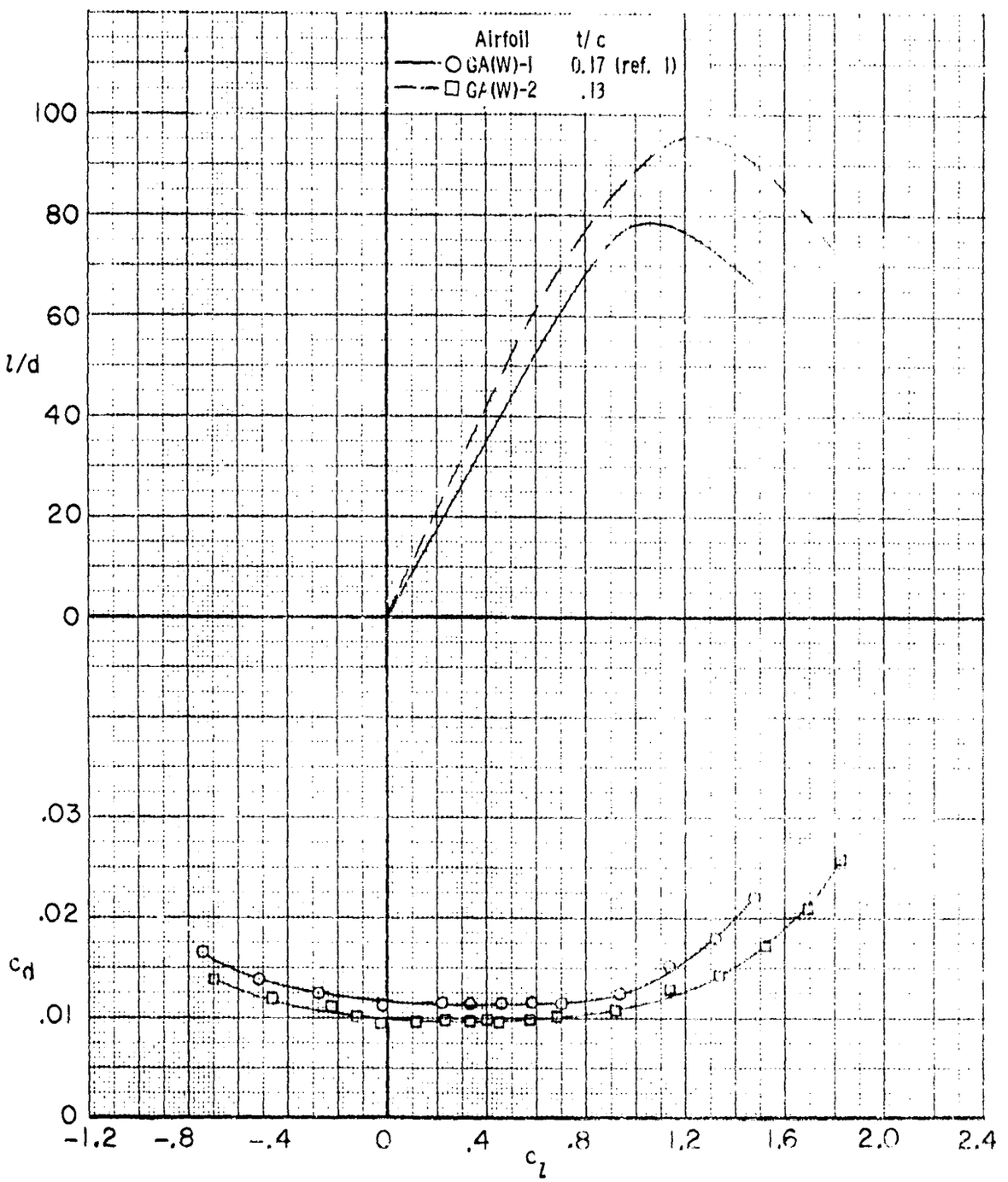

(b) $R = 4.3 \times 10^6$. Concluded.

Figure 10. - Continued.

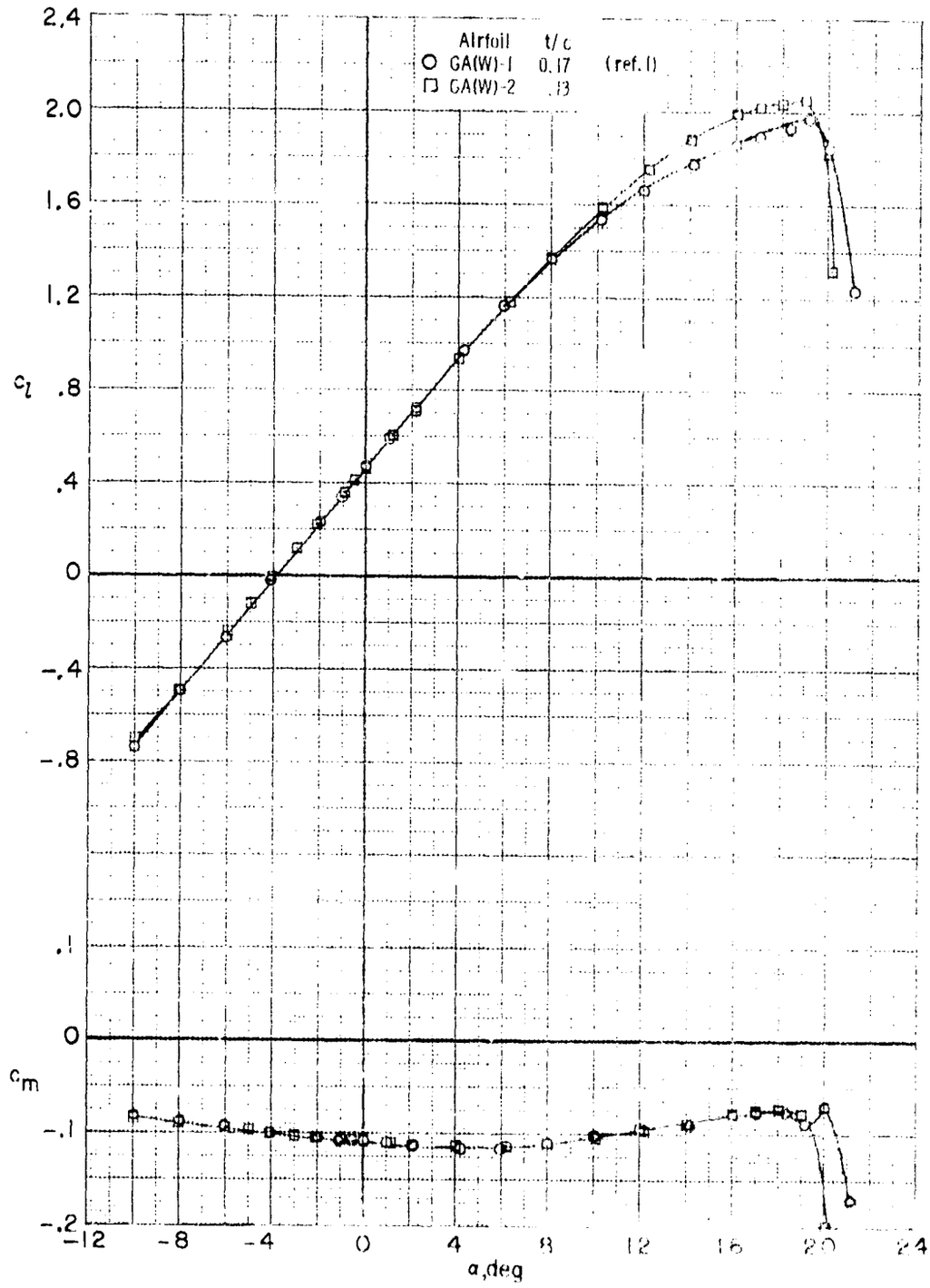

(c) R = 6.3 x 10^6.

Figure 10. - Continued.

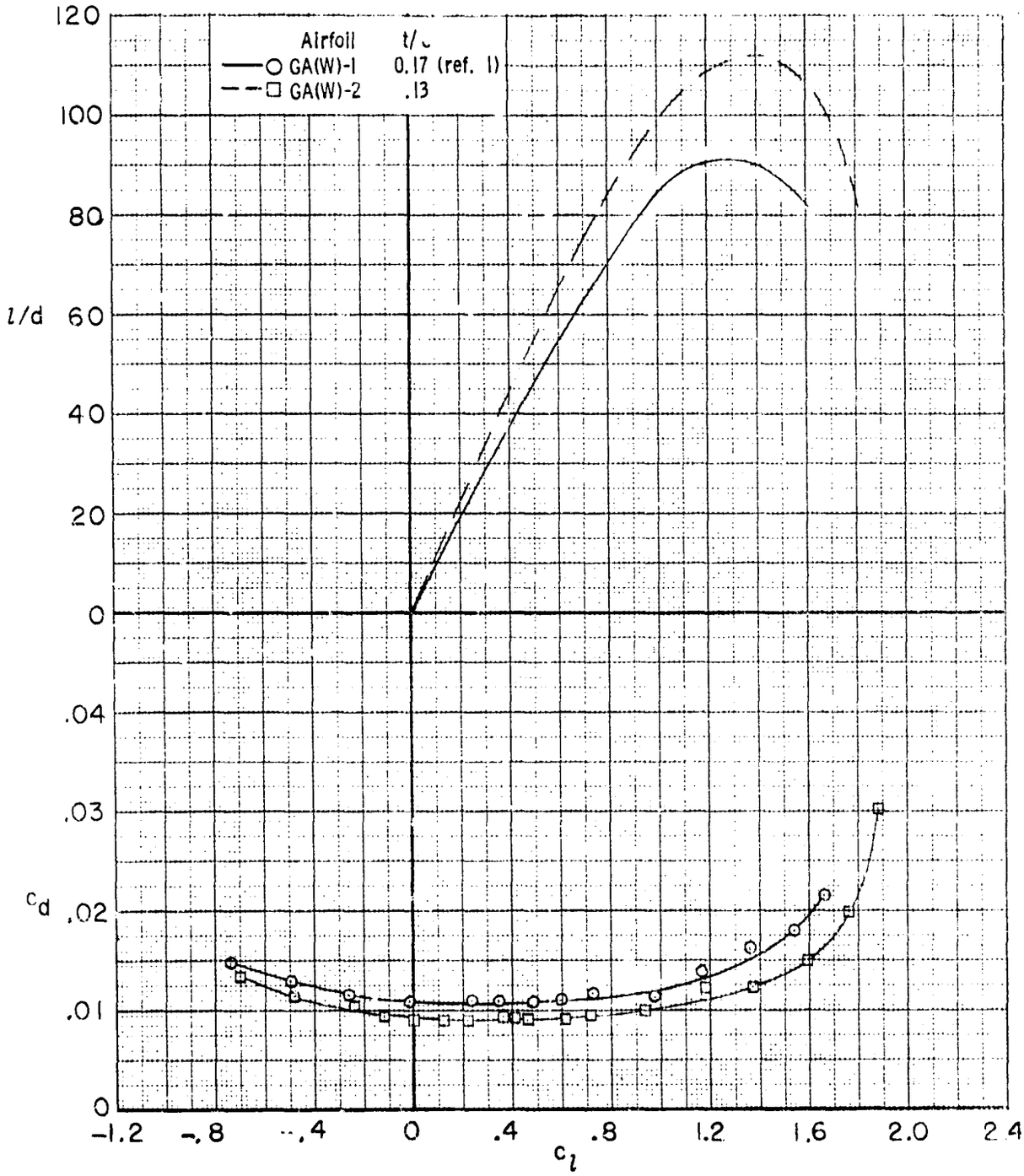

(c) R = 6.3 x 10^6. Concluded.

Figure 10. - Concluded.

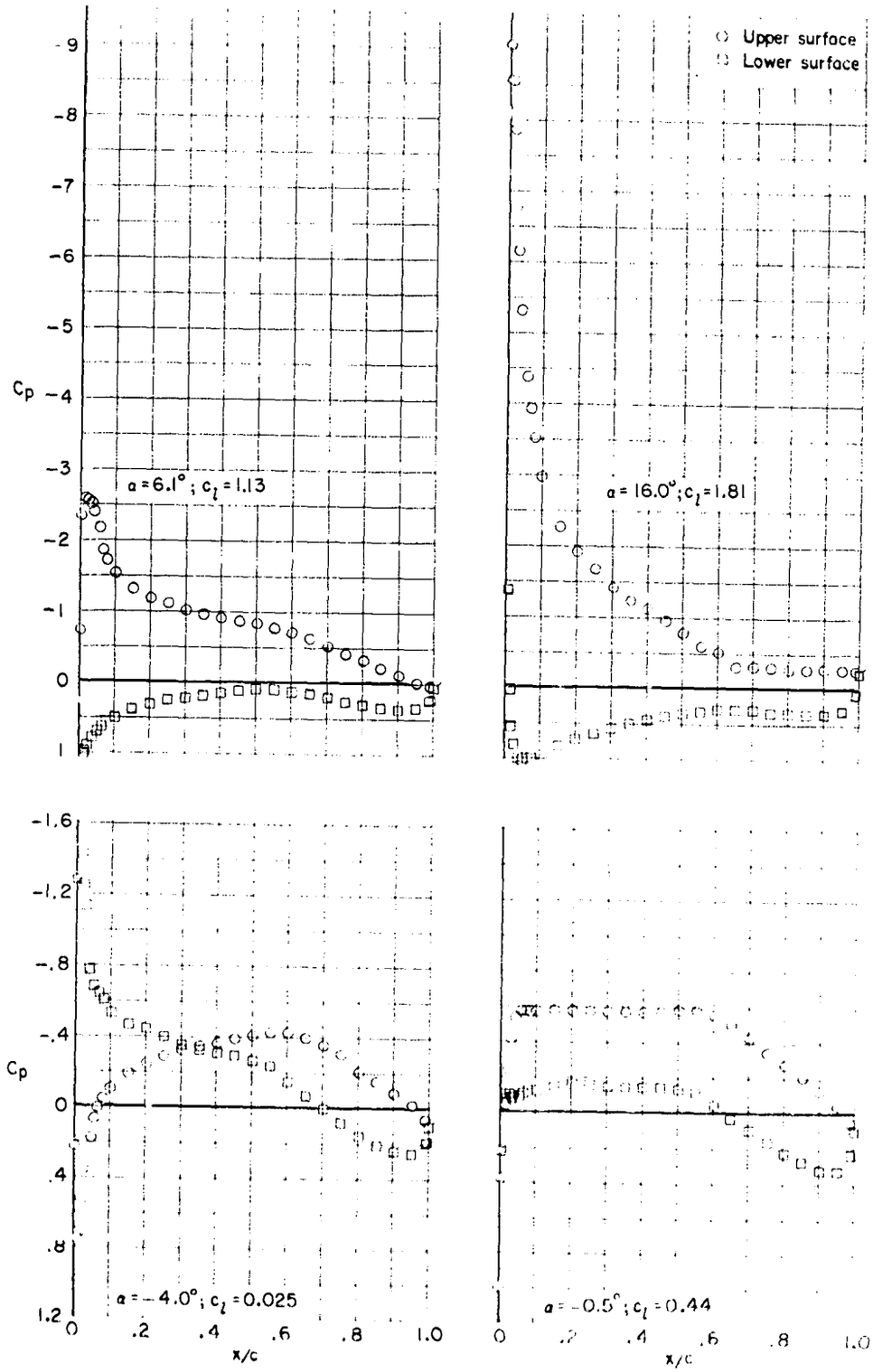

Figure 11. - Typical chordwise pressure distributions for NASA GA(W)-2 airfoil. M = 0.15; R = 3.0 x 10^6; airfoil smooth. (Flagged symbol indicates base pressure orifice).

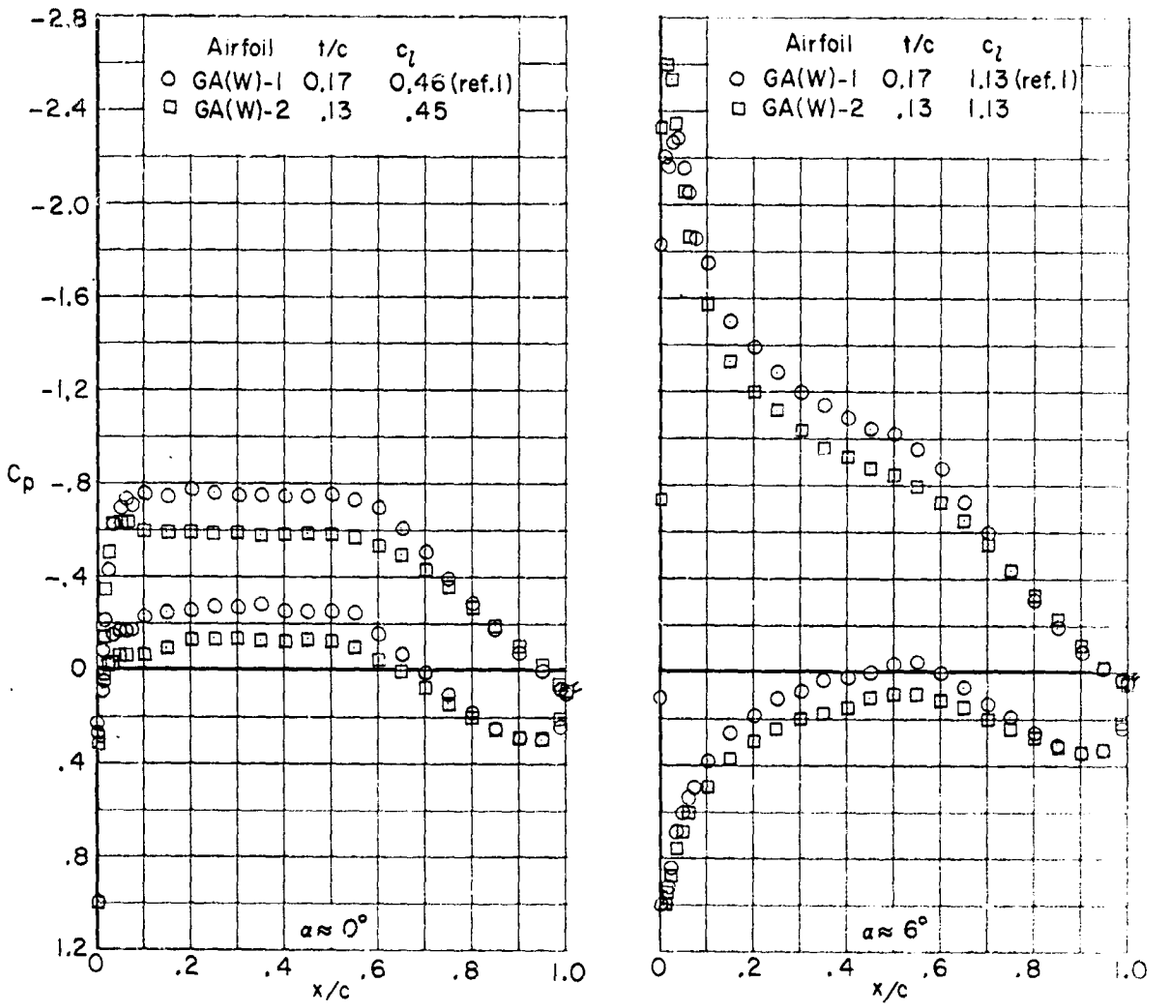

(a) $\alpha \approx 0°$ and 6°.

Figure 12.- Comparison of the chordwise pressure distributions for the NASA GA(W)-1 and GA(W)-2 airfoils. $M = 0.15$; $R = 4.3 \times 10^6$; transition fixed at $x/c = 0.075$. (Flagged symbols indicate base pressure orifice).

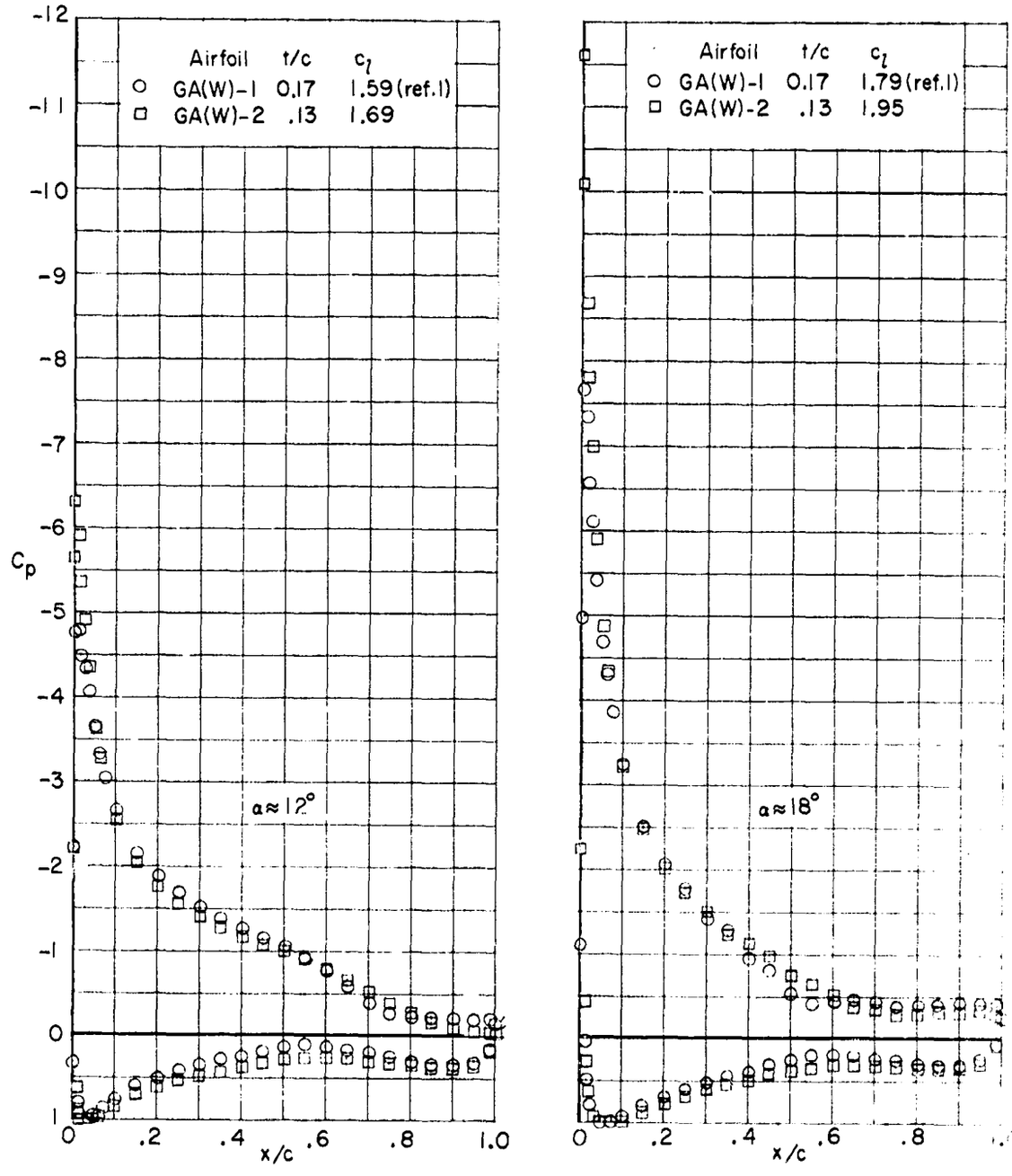

(b) $\alpha \approx 12°$ and 18°.

Figure 12. - Concluded.

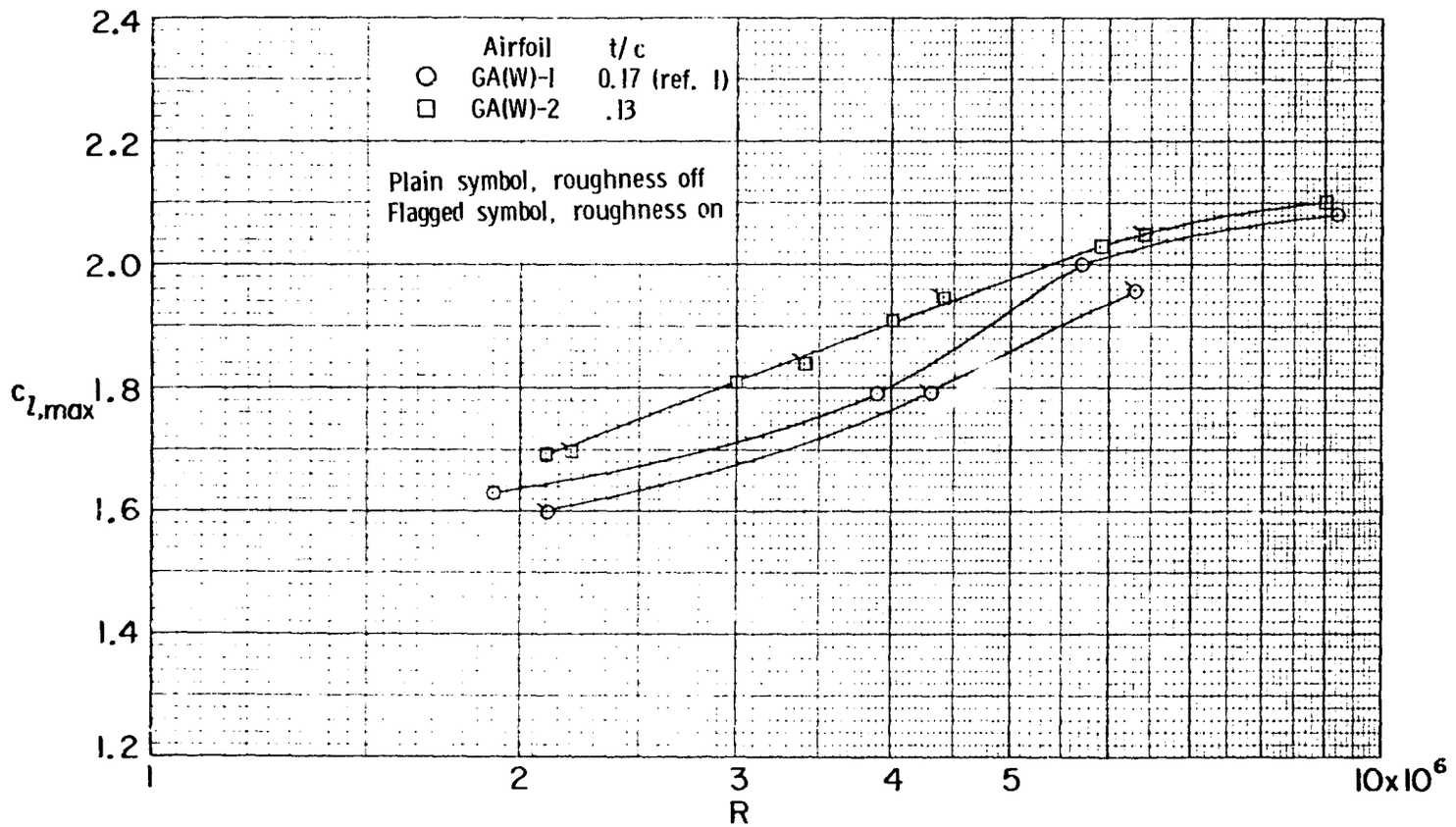

Figure 13.- Variation of maximum section lift coefficient with Reynolds number for GA(W)-1 and GA(W)-2 airfoils. M = 0.15.

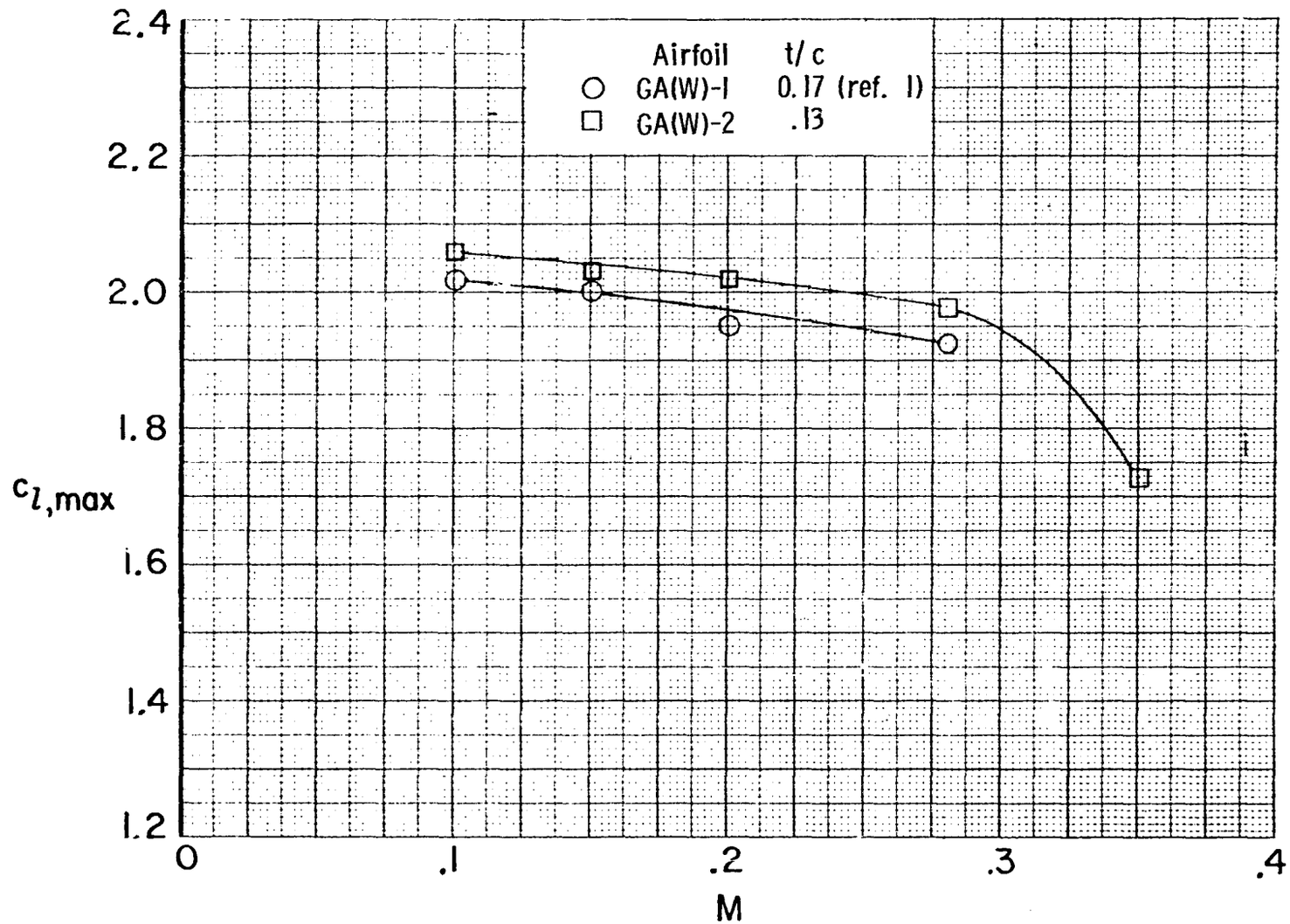

Figure 14.- Variation of maximum section lift coefficient with Mach number for GA(W)-1 and GA(W)-2 airfoils. $R \approx 6.0 \times 10^6$; airfoils smooth.

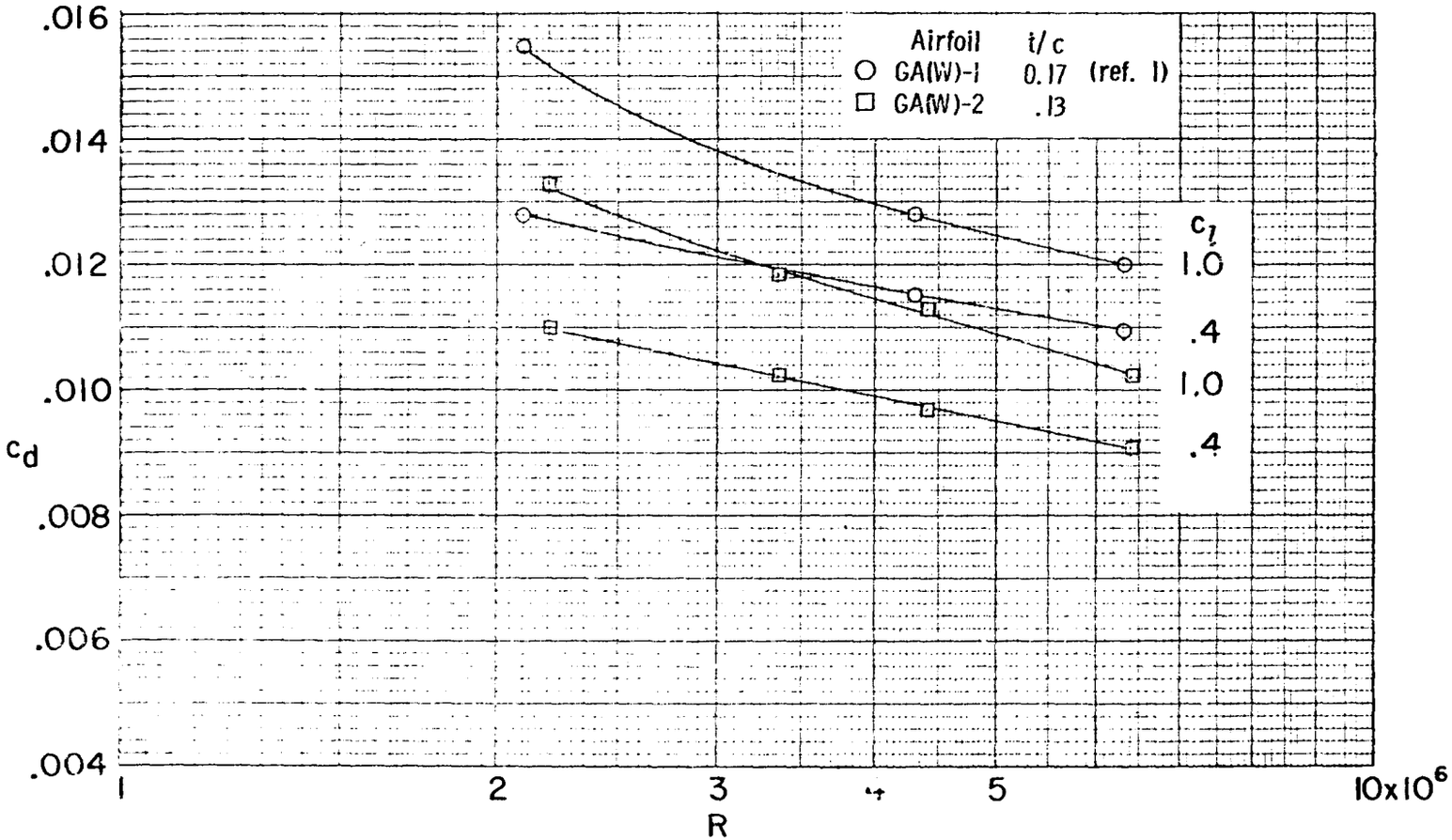

Figure 15.- Variation of drag coefficient with Reynolds number for GA(W)-1 and GA(W)-2 airfoils. M = 0.15; transition fixed at x/c = 0.075.

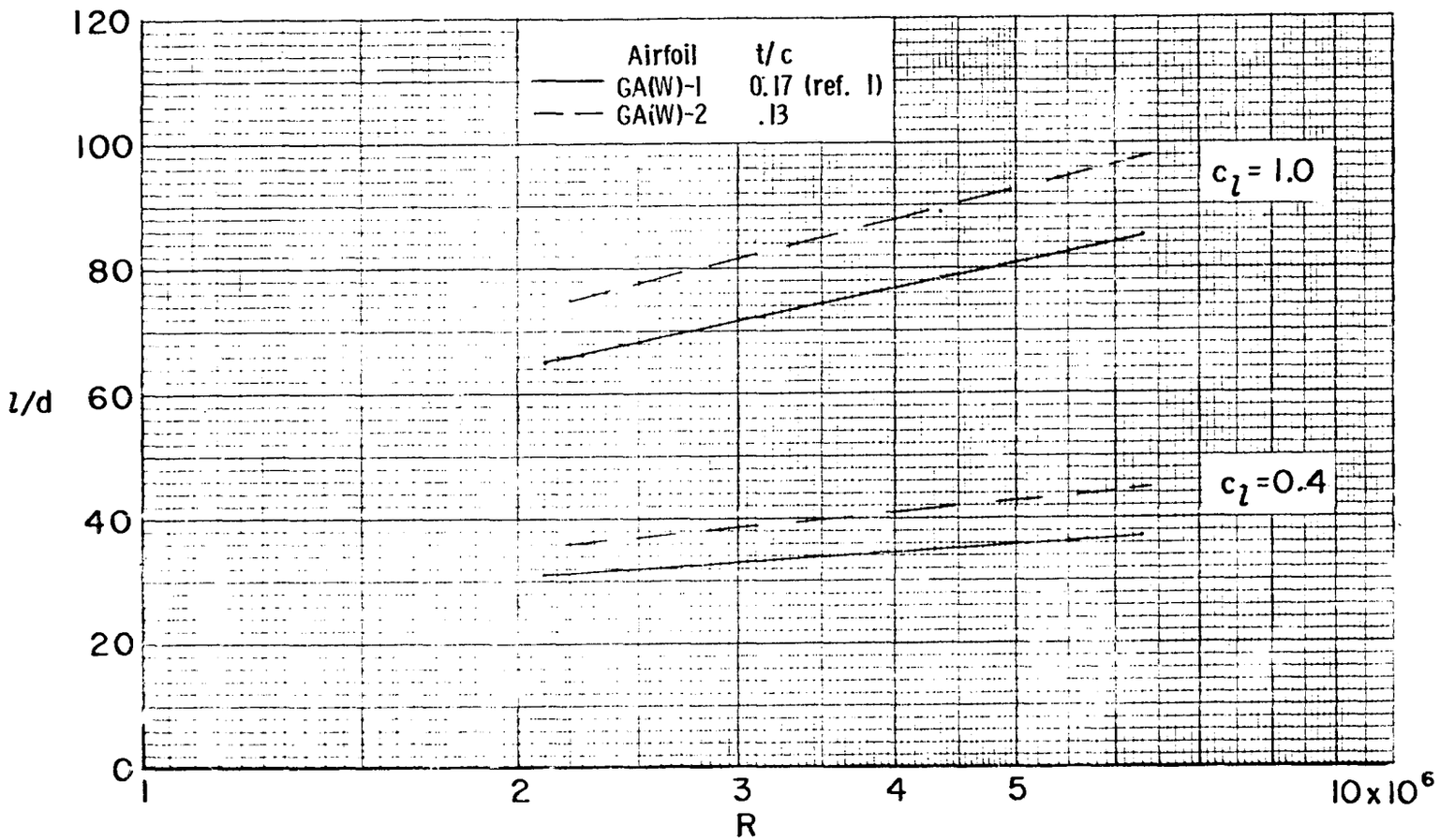

Figure 16.- Variation of lift-drag ratio with Reynolds number for GA(W)-1 and GA(W)-2 airfoils. M = 0.15; transition fixed at x/c = 0.075.

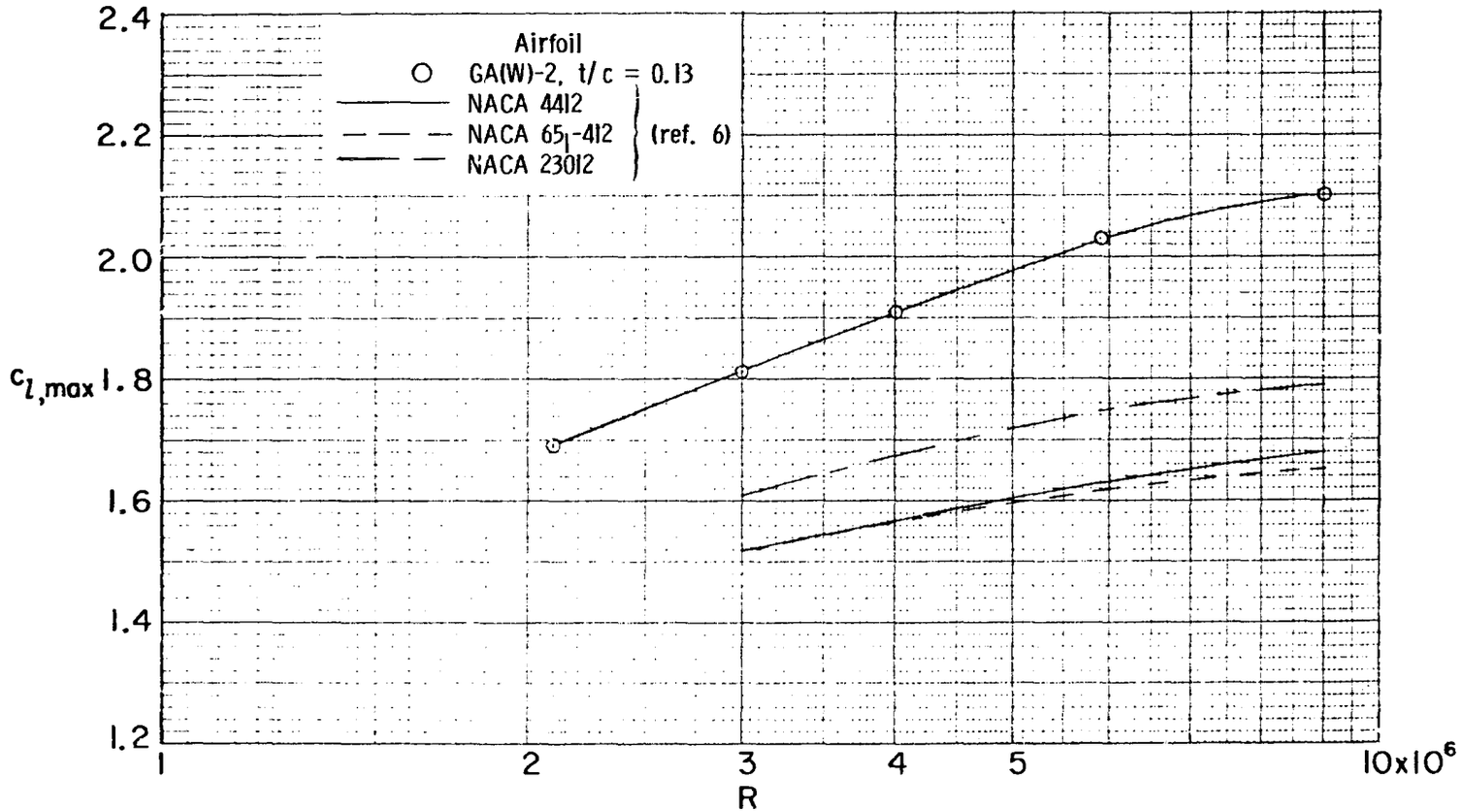

Figure 17.- Variation of maximum section lift coefficient with Reynolds number for various airfoils. M = 0.15; airfoils smooth.

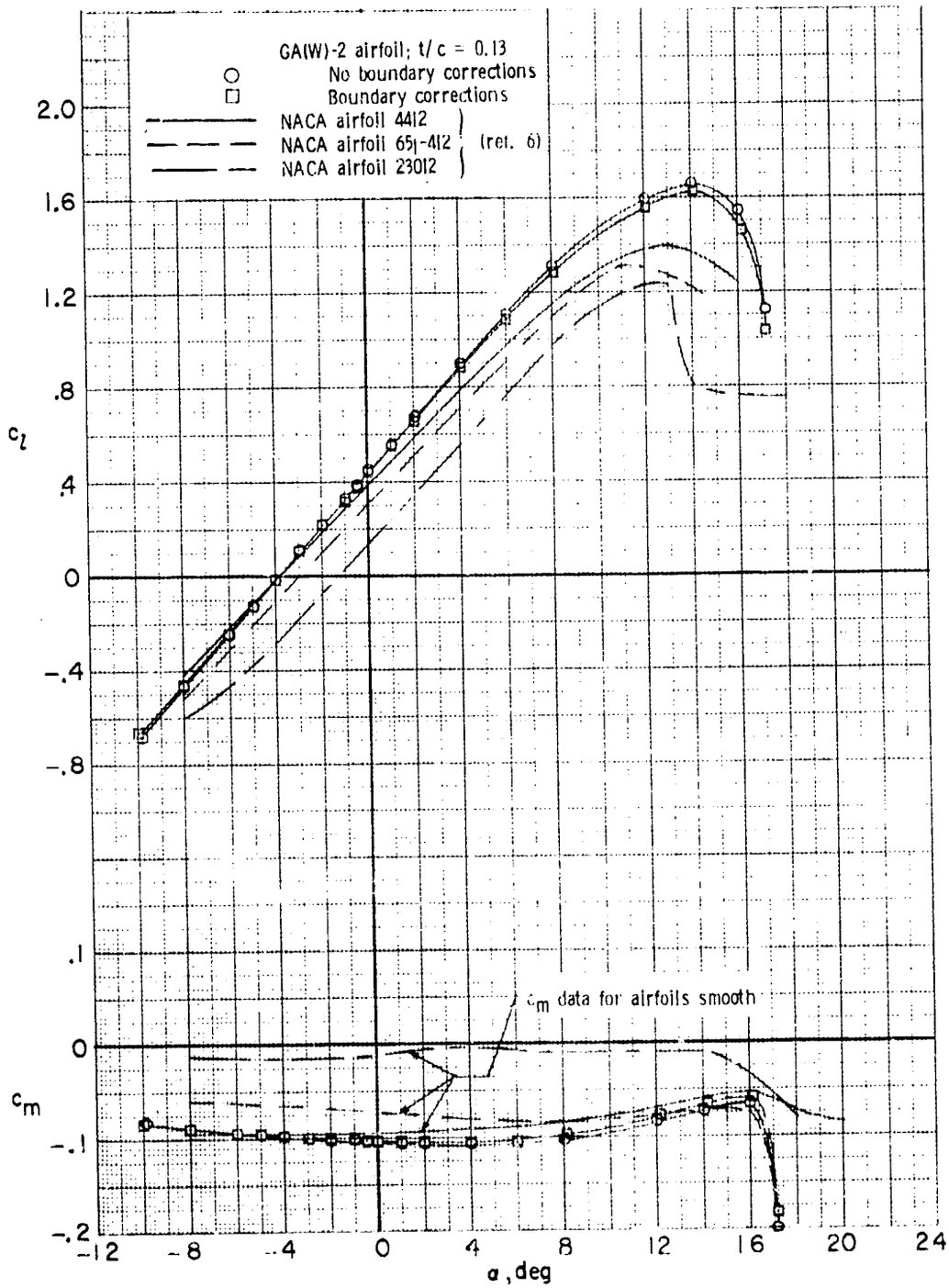

(a) Lift and moment data.

Figure 18. - Comparison of section characteristics of NASA GA(W)-2 airfoil and NACA 4412, 23012, and 65₁-412 airfoils. M = 0.15; R = 6.0 x 10^6; wrap-around roughness to 0.08c surface length (no. 60 grit).

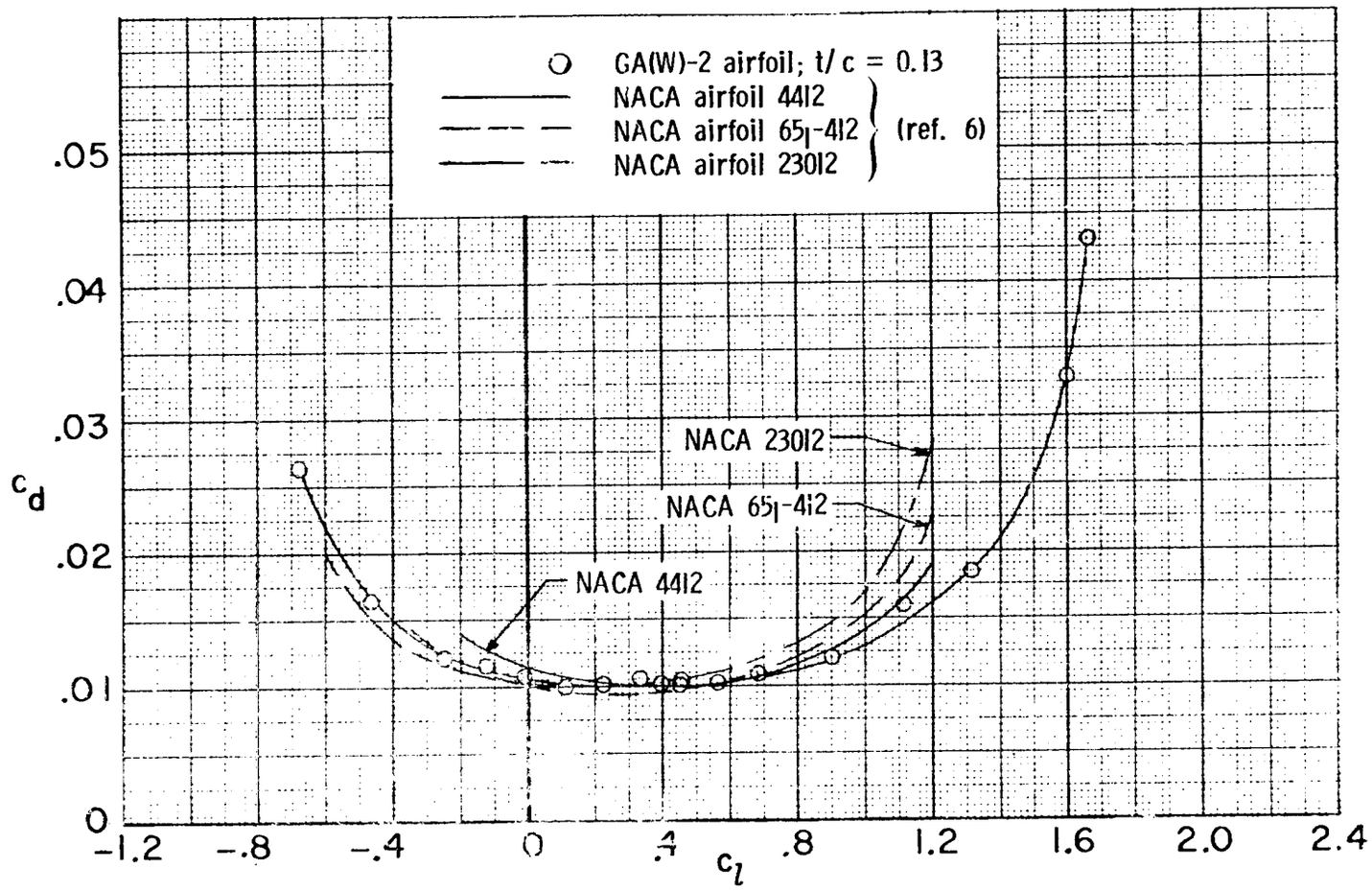

(b) Drag polars.

Figure 18. - Concluded.

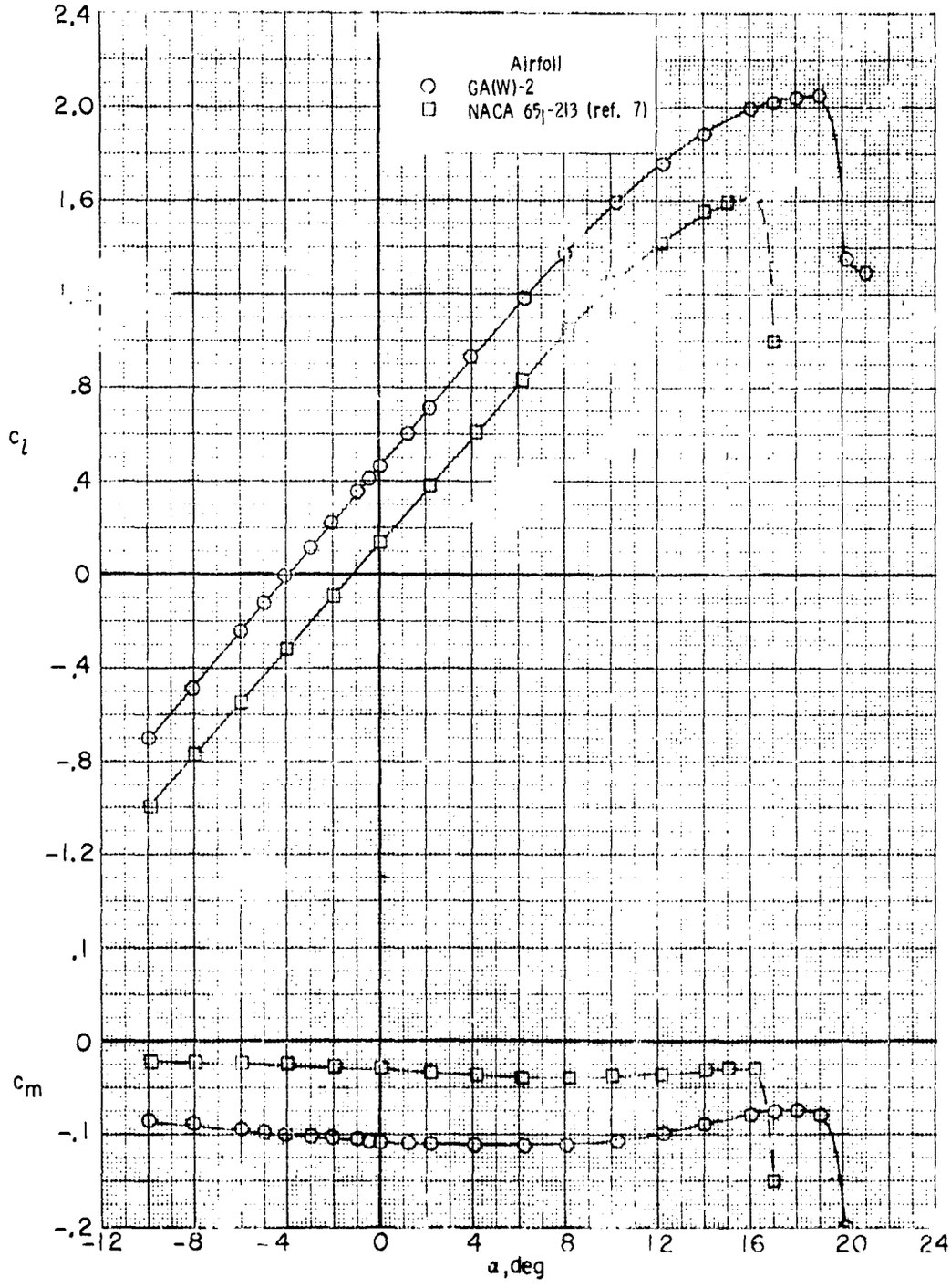

(a) Lift and moment data.

Figure 19.- Comparison of section characteristics of NASA GA(W)-2 and NACA 65$_1$-213 airfoils. M = 0.15; R ≈ 6.0 x 10^6; strip roughness.

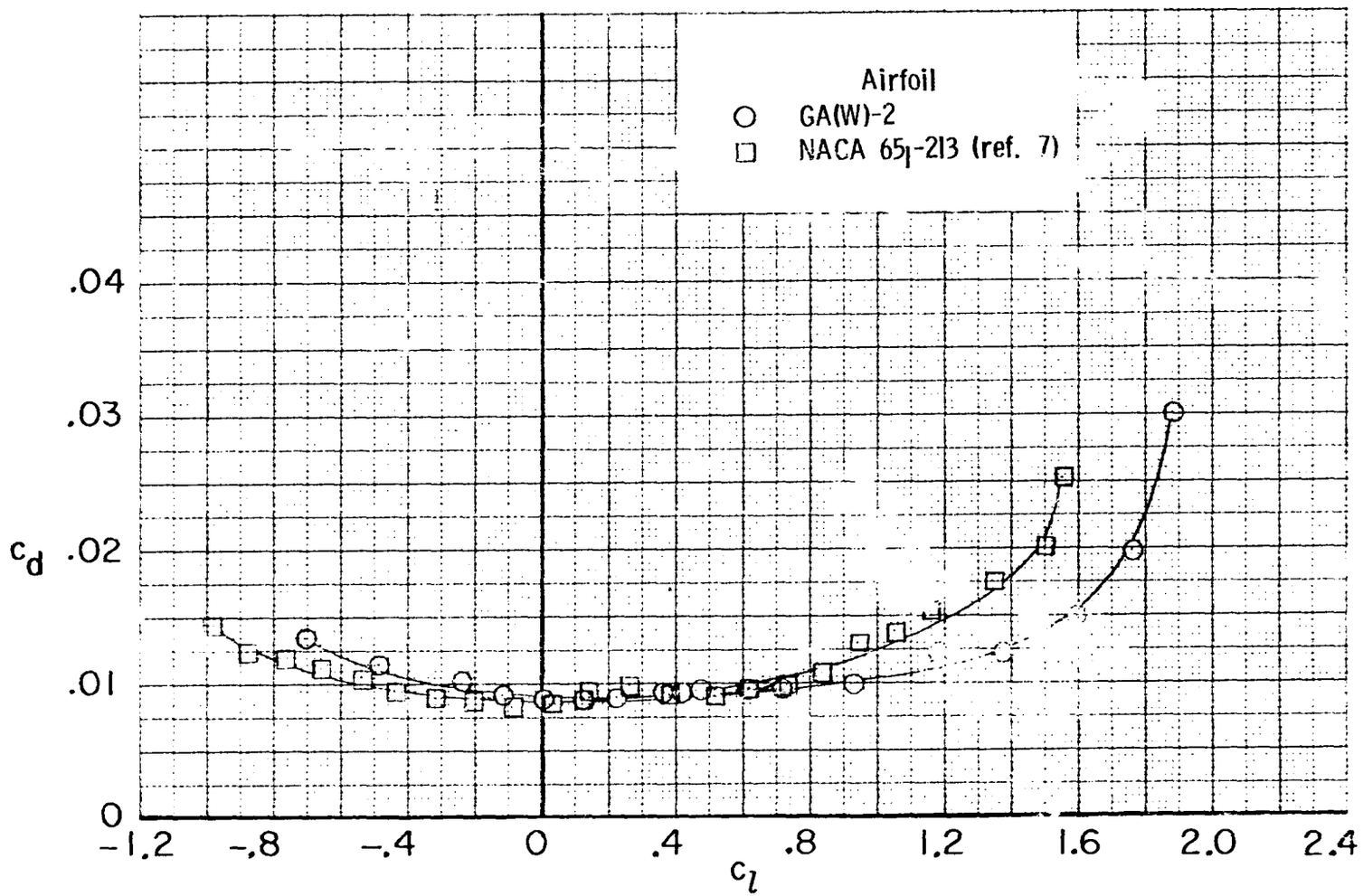

(b) Drag polars.

Figure 19. - Concluded.

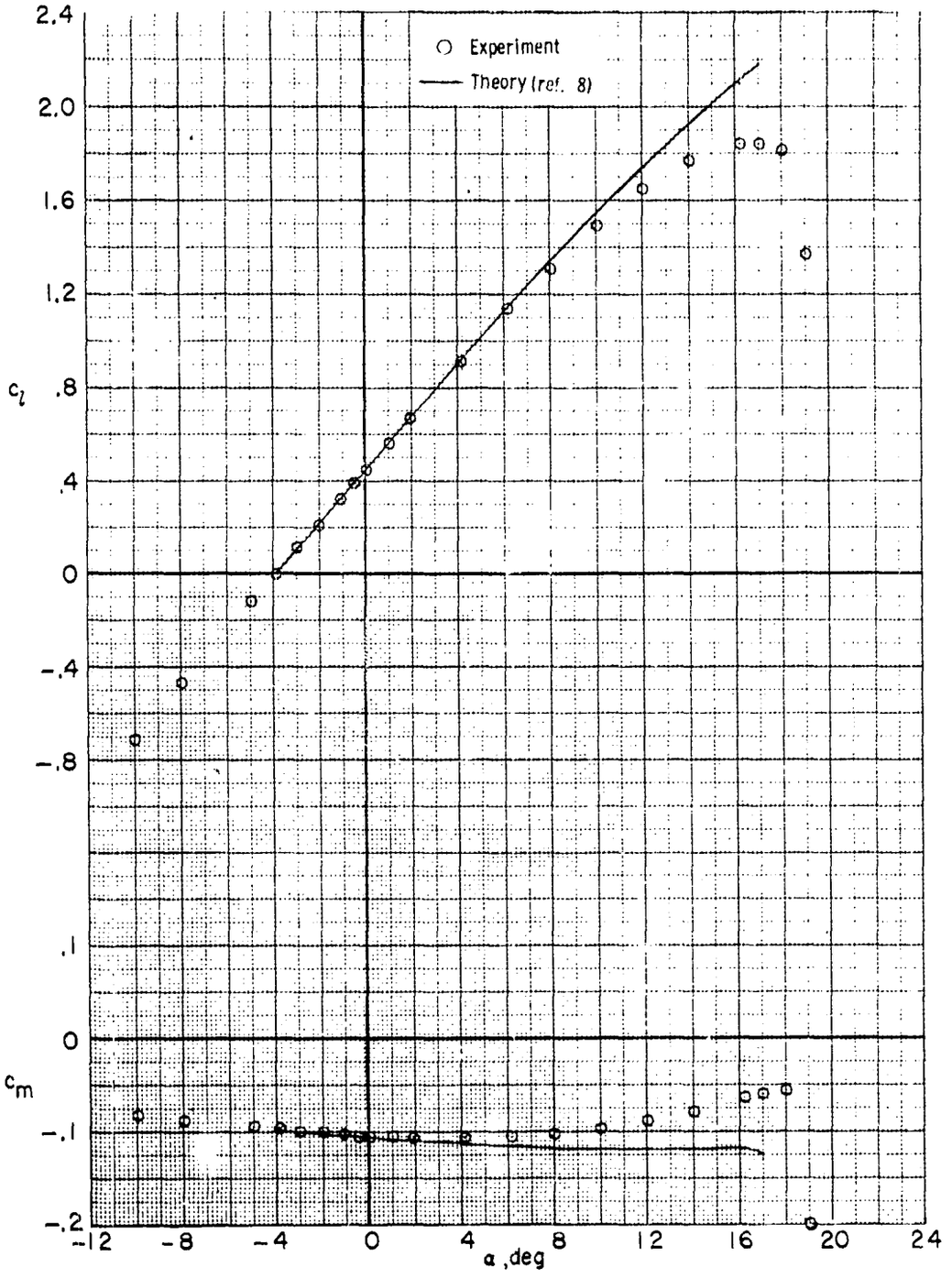

Figure 20. - Comparison of experimental and theoretical section characteristics for the NASA GA(W)-2 airfoil. M = 0.15; R = 3.0 x 10^6; transition fixed at x/c = 0.075.